CONFINEMENT AND β_p-STUDIES IN NEUTRAL INJECTION HEATED ASDEX PLASMAS

F.Wagner, G.Becker, K.Behringer, D.Campbell, A.Eberhagen, W.Engelhardt, G.Fußmann, O.Gehre, J.Gernhardt, G.v.Gierke, G.Haas, M.Huang+, F.Karger, M.Keilhacker, O.Klüber, M.Kornherr, K.Lackner, G.Lisitano, G.G.Lister, H.M.Mayer, D.Meisel, E.R.Müller, H.Murmann, H.Niedermeyer, W.Poschenrieder, H.Rapp, H.Röhr, F.Schneider, G.Siller, E.Speth, A.Stäbler, K.H.Steuer, S.Succi, G.Venus and O.Vollmer

IPP III/86 March 1983

MAX-PLANCK-INSTITUT FÜR PLASMAPHYSIK

8046 GARCHING BEI MÜNCHEN

MAX-PLANCK-INSTITUT FÜR PLASMAPHYSIK

GARCHING BEI MÜNCHEN

CONFINEMENT AND β_p-STUDIES IN NEUTRAL INJECTION HEATED ASDEX PLASMAS

F.Wagner, G.Becker, K.Behringer, D.Campbell,
A.Eberhagen, W.Engelhardt, G.Fußmann, O.Gehre,
J.Gernhardt, G.v.Gierke, G.Haas, M.Huang+,
F.Karger, M.Keilhacker, O.Klüber, M.Kornherr,
K.Lackner, G.Lisitano, G.G.Lister, H.M.Mayer,
D.Meisel, E.R.Müller, H.Murmann, H.Niedermeyer,
W.Poschenrieder, H.Rapp, H.Röhr, F.Schneider,
G.Siller, E.Speth, A.Stäbler, K.H.Steuer,
S.Succi, G.Venus and O.Vollmer

IPP III/86 March 1983

+Academia Sinica, Peking, The Peoples' Republic of China

Die nachstehende Arbeit wurde im Rahmen des Vertrages zwischen dem Max-Planck-Institut für Plasmaphysik und der Europäischen Atomgemeinschaft über die Zusammenarbeit auf dem Gebiete der Plasmaphysik durchgeführt.

CONFINEMENT AND β_p-STUDIES IN NEUTRAL INJECTION HEATED ASDEX PLASMAS

F.Wagner, G.Becker, K.Behringer, D.Campbell, A.Eberhagen, W.Engelhardt, G.Fußmann, O.Gehre, J.Gernhardt, G.v.Gierke, G.Haas, M.Huang+, F.Karger, M.Keilhacker, O.Klüber, M.Kornherr, K.Lackner, G.Lisitano, G.G.Lister, H.M.Mayer, D.Meisel, E.R.Müller, H.Murmann, H.Niedermeyer, W.Poschenrieder, H.Rapp, H.Röhr, F.Schneider, G.Siller, E.Speth, A.Stäbler, K.H.Steuer, S.Succi, G.Venus and O.Vollmer.

Max-Planck-Institut für Plasmaphysik, EURATOM-Association
D-8046 Garching

Abstract

Neutral injection experiments into limiter and divertor discharges in ASDEX are described with hydrogen and deuterium as working gas. Two operational regimes have been observed in neutral injection heated divertor discharges. One regime is characterized by deteriorated energy and particle confinement. The global energy confinement times are comparable to those of neutral injection heated limiter discharges. The other regime has particle and energy confinement times comparable to those of ohmic discharges with τ_E = 40 - 60 msec at beam powers up to 3.1 MW. This regime is further characterized by high β_p-values comparable to the aspect ratio A ($\beta_p \sim 0.65\,A$), by good electron heating ($\eta_e \sim 2.5 \times 10^{13}$ eV cm^{-3} kW^{-1}) and ion heating ($\eta_i \sim 4.2 \times 10^{13}$ eV cm^{-3} kW^{-1}). In both regimes, τ_E increases with plasma current but there is hardly any variation with density. The differences in confinement and scaling to ohmic discharges seem to be caused by modifications of the electron loss channel. The high β_p-regime develops at an injection power $\geq$1.8 MW, $\bar{n}_e \geq 3 \times 10^{13}$cm^{-3} and $q \geq 2.45$, and is so far only observed in divertor discharges. There are indications that this may be due to the broad profiles with high edge temperatures which can develop in divertor discharges. An indication of broad current density profiles is given by the lack of sawtooth activity in these discharges.

+On leave from Academia Sinica, Peking, The Peoples' Republic of China

1. Introduction

Extensive studies have been made of plasma heating and confinement in the ASDEX tokamak with intense neutral beam injection (NI). The effect of NI is illustrated in Fig. 1, which shows the rise of the central ion and electron temperature, $T_i(0)$ and $T_e(0)$, with 2.61 MW NI power into a medium density discharge. $T_i(0)$ approaches 5 keV.

ASDEX /1/ is a large divertor tokamak, which can be operated in different poloidal divertor configurations. For reasons of comparison, ASDEX was also operated with a classical material limiter. The geometrical parameters of ASDEX are: R = 165 cm and a = 40 cm. Typically, ASDEX is operated at B_T = 2.2 T and a plasma current between 200 and 400 kA.

The NI system of ASDEX /2/ is presently capable of injecting 3.1 MW for 200 msec at a source voltage of 40 kV. The power is delivered by two beam lines each housing four individual sources. Both beam lines are oriented tangentially, at a tangency radius of 140 cm. The ion sources are exclusively run with hydrogen, but NI is carried out either into hydrogen (H^+) or deuterium (D^+) plasmas. The power P_{NI} into the vacuum vessel is reduced owing to losses in the beam duct, which amount to maximally 15%. P_{NI} can accurately be measured by shooting the beams, during an ohmic discharge, onto retractable calorimeters located within the vacuum vessel in the space between plasma and wall. Thereby, P_{NI} is measured with all stray fields present (apart from the actual vertical field which increases during the NI pulse owing to the higher β_p).

The power P_{abs} which is actually absorbed by the plasma is lower than P_{NI} by shine-through, bad orbit and charge exchange losses of beam ions. P_{abs} is calculated from P_{NI} using a beam deposition code /3/.

An important diagnostic tool for the characterization of high power NI heated plasmas is the measurement of $\beta_p + l_i/2$ (l_i = internal inductance) from the plasma equilibrium, and $\beta_{p\perp}$ deduced from the plasma diamagnetic effect. As these quantities are frequently used in this paper, it seems to be justified to describe briefly the technical set-up and characterize the reliability tests.

$\beta_p + \frac{l_i}{2}$ is determined from the Shafranov equation either using the magnetic field and flux signals from probes located within the plasma vessel or by calculating the vertical field directly from the vertical field coil current. This is reasonable in the case of ASDEX with its good stray field compensation and with a rather homogeneous vertical field distribution. The agreement between the two measurements of $\beta_p + \frac{l_i}{2}$ is in the average 3%. Thus, falsified measurements due to stray field or eddy current contributions to the plasma equilibrium can largely be excluded.

The diamagnetic loop and the necessary compensating loop, which measure the toroidal flux, are mounted onto a frame outside of the vacuum vessel. Several pre cautions are taken to reduce the effect of toroidal stray fields /4/. First, the loop is located at a toroidal position far away from the current leads to ohmic heating, vertical or radial field, or to the divertor coils. Also the lack of an iron core transformer prevents excessive field distortions. The diamagnetic loops are aligned in a plane perpendicular to the axis of the vacuum vessel with an accuracy of 1 mm per mtr. The induced stray field signals of all poloidal coils are measured independently, without plasma, at coil currents corresponding to the values during an actual discharge. The stray field signals cancel each other partly. The amplitude is less than 10% of the signal during an ohmic discharge. In order to reduce it further, the current of each poloidal coil is measured individually and fed into a compensating electronic system. By this technique, the stray field contributions are nulled. The amount of misalignment, with respect to the plasma current, has been checked by two subsequent plasma shots with reversed toroidal

field directions but otherwise identical plasma parameters. The observed difference in the absolute value of the diamagnetic signal is 25% and has also been compensated as described above.

Finally, the radial movement (contraction) of vacuum vessel and diamagnetic loops, which gives rise to a 5% change in the diamagnetic signal, is corrected by the analysis program which calculated $\beta_{p\perp}$. With these measures, the error in $\beta_{p\perp}$ is less than 0.1 and largely independent of $\beta_{p\perp}$.

The general agreement of the β_p-values deduced from plasma equilibrium, plasma diamagnetism and from measured density (interferometer) and temperature (CX, ECE) profiles can be illustrated by an ohmic discharge (to avoid problems arising from an isotropic plasma pressure) with I_p = 250 kA, B_T = 22 kG and $\bar{n}_e = 3{\cdot}7 \times 10^{13} cm^{-3}$. $\beta_p + \frac{l_i}{2} = 1.02$ from the Mirnov probes and 1.07 from the vertical field which give β_p = 0.25 and 0.30 respectively (l_i = 1.535, derived from q_a = 4.38). $\beta_{p\perp}$ from the diagmagnetic signal is 0.30 and from profile measurements β_p = 0.34.

2. NI into Hydrogen or Deuterium Plasmas

It is well documented for ohmically heated discharges /5/ that particle and energy confinement times are longer in deuterium than in hydrogen plasmas. Figure 2 recapitulates this in a diagram, which shows the increase of $\beta_{p\perp}$ and in energy confinement time τ_E^+ (deduced from $\beta_{p\perp}$) at the transition from hydrogen to deuterium as working gas. The last hydrogen discharge was shot # 7888. The exchange of gas deposited into the walls occurs within a few shots with the divertor configuration. With deuterium, $\beta_{p\perp}$ is higher by ~ 30% which corresponds to an increase in energy confinement time τ_E^+, from 53 msec in hydrogen to 77 msec in deuterium. The ratio of the τ_E^+-values is 1.45.

Figure 3 shows the increase in $\beta_p + l_i/2$ and $\beta_{p\perp}$ with NI into hydrogen and deuterium plasmas at different plasma currents and

configurations. The increase in $\beta_p + \frac{l_i}{2}$ with P_{NI} reflects mostly an increase in β_p because l_i is found not to change very much. (In limiter discharges sawtooth fluctuations in the plasma center are still present up to the highest injection powers. A slight reduction in l_i particularly in divertor discharges cannot be excluded because the T_e-profiles tend to broaden. An increase in l_i, however, is necessary to contribute to the rise of $\beta_p + \frac{l_i}{2}$. A dominant contribution of l_i requires a dramatic peaking of the current distribution which is unlikely.)

In all cases shown in Fig. 3, β_p increases linearly with P_{NI} without any indication of saturation at high power levels as observed with other tokamaks /6/. But there is a clear difference in slope of β_p vs. P_{NI} between hydrogen and deuterium. As in the ohmic case, β_p is higher in deuterium than in hydrogen plasmas.

The difference in $\Delta(\beta_p + \frac{l_i}{2})$ and $\Delta\ \beta_{p\perp}$ is mostly caused by plasma rotation and the beam contribution to β_p which - in case of tangential injection - influences the plasma equilibrium more than the plasma diamagnetism. The beam contribution to β_p, deduced from the comparison between equilibrium and diamagnetic β_p, agrees fairly well with the code calculation. Because of the kinetics in the slowing down process, the beam contribution to β_p is higher in deuterium than in hydrogen typically by 0.05.

But the difference in $\Delta(\beta_p + \frac{l_i}{2})$ between D^+ - and H^+ -plasmas, as shown in Fig. 3, is too big to be explained by the beam contribution alone. As in the ohmic case, the discrepancy reflects mostly a difference in the confinement properties. This is also born out by the variation of $T_e(0) \times \bar{n}_e$ with P_{NI}. $T_e(0) \times \bar{n}_e$ is an easily accessible measure of the electron energy content with $T_e(0)$ determined by ECE and $\bar{n}_e$ by HCN-interferometry. $T_e(0) \times \bar{n}_e$ is higher in D^+ than in H^+ plasmas indicating that the difference in β_p is mostly a bulk plasma property. The maintenance of the better confinement properties of deuterium with NI is remarkable because, with hydrogen injection into D^+-plasmas, the plasma becomes a mixture of H^+ and D^+ with a 1:1 composition at high injection power into a medium density discharge.

3. NI into Material Limiter Discharges

Neutral injection was carried out into limiter discharges with two different limiter configurations

- a toroidal limiter mounted at the bottom side of the plasma; the limiter was toroidally closed /7/;
- a poloidal wing limiter /1/.

In both cases the limiter material was carbon.
The two limiters are sketched in Fig. 4 in a poloidal cross-section together with the circular plasma. The dashed contours outline the separatrices of the divertor configurations, possible with each limiter. The toroidal limiter only allowed single-null divertor discharges where the magnetic axis was moved upward by ΔZ (typically 4 cm) by a radial magnetic field. In the case of the poloidal limiter, double null divertor configurations are possible with the multipoles activated and the limiter wings moved to the wall.

The advantage of this toroidal limiter is that the plasma can freely increase and shrink in major radius (like in the divertor configuration) without having inner magnetic surfaces intersect the limiter. Such a variation in major radius occurs as soon as the NI beams are switched on or off because of the contribution of the beam pressure to the plasma equilibrium conditions. The amplitudes of these excursions depend on beam power and the response time of the vertical field feedback system. (An example of the radial movement of the plasma column due to the NI beams is given in Fig. 23).

With the poloidal limiter as an obstacle against this movement, the plasma cross-section is reduced during the initial and final phases of NI and the movement of the plasma might cause a more violent plasma limiter interaction. A remedy to this lack of stability is to work with a vertical field variation pre-programmed to match the expected effect of NI on the plasma position (feed forward).

The linear increase in $\Delta(\beta_p + \frac{1}{2} l_i)$ or $\Delta \beta_{p\perp}$, respectively, of limiter discharges due to NI has already been documented in Fig. 3. The difference in absolute value between poloidal and toroidal limiter discharges is due to the different plasma currents and not correlated with the limiter configuration.

An important criterion for future plasma devices and fusion reactors is the variation of the global energy confinement time τ_E at high injection power and at high levels of plasma energy and β_p. In Fig. 5, τ_E^+ is plotted versus P_{NI}. τ_E^+ is deduced from the diamagnetically measured $\beta_{p\perp}$. With tangential injection, $\beta_{p\perp}$ represents more the thermal energy content of the plasma compared to β_p from the plasma equilibrium, which contains the beam contribution.

τ_E^+ for the two limiter configurations (although at different plasma currents) and for hydrogen and deuterium discharges with the toroidal limiter are compared. The general tendency of τ_E^+ is to decrease with increasing NI power to values which are far below the ohmic values. An injection power equivalent to the ohmic input ($P_{NI} \cong 0.3$ MW) is sufficient to significantly reduce τ_E^+. With $P_{NI} = 0.6$ MW, τ_E^+ has already reached the low level of confinement characteristic of NI heated tokamak plasmas. Increasing the power beyond this level causes only a moderate further decrease in confinement time[x].

As already indicated in Fig. 3 and as in the ohmic heating phase with NI also, τ_E^+ is higher with deuterium than hydrogen as working gas. In the plateau phase of τ_E^+ vs. P_{NI}, the ratio of the confinement times is 1.3. As in Fig. 3, the higher confinement time with poloidal compared to toroidal limiter discharges is not a consequence of the different limiter configurations but is caused by the

---

[x] It requires only a simple consideration, to realize, that a linear increase in $\Delta \beta_{p\perp}$ with P_{NI} is in agreement with the variation of τ_E^+ as shown in Fig. 5:

$$\tau_E^+(NI) = C_1 \frac{\beta_p(OH) + \Delta \beta_{p\perp}}{P_{abs} + U \cdot I} = C_1 \frac{\beta_p(OH) + C_2 P_{NI}}{C_3 P_{NI} + (P_{OH} - C_4 P_{NI})} = \tau_E^+(OH) \frac{1 + \alpha x}{1 + \beta x}$$

with $x = P_{NI}/P_{OH}$ and $\beta > \alpha$. U and I are loop voltage and plasma current, $C_{1 \ldots 4}$ are constants.

difference in plasma current. Contrary to the ohmic phase, with NI the energy confinement time increases with plasma current.

Figure 6 shows the variation of τ_E^+ with line averaged density $\bar{n}_e$ of ohmically and NI heated limiter plasmas. The increase in confinement time with density is a well documented experimental result of ohmically heated plasmas /8/. The increase in τ_E, which is caused by a corresponding decrease in electron thermal transport, continues till the ion losses contribute to the global plasma losses. From there on, τ_E is independent of $\bar{n}_e$ in ohmic plasmas.

With NI, we find no density dependence of τ_E^+ in the density range $2 \times 10^{13} \leq \bar{n}_e \leq 5 \times 10^{13} cm^{-3}$. The lack of density dependence is first documented by Fig. 7 which shows the variation of $\beta_p + l_i/2$ during a NI pulse with an increasing density. Apart from the initial increase due to NI, $\beta_p + l_i/2$ does not further rise with density. The τ_E^+ -data, shown in Fig. 6, are taken during stationary phases of NI into hydrogen and deuterium plasmas. With NI the lack of density dependence is not caused by the neoclassical ion contribution to the global energy confinement as in the ohmic case. In the density range of the present investigations, the power loss is predominantly through the electron channel /9/ and the lack of density dependence of τ_E^+ points toward a modified electron thermal transport.

4. NI into Divertor Discharges

With NI into divertor plasmas, two types of discharges are observed /10/. The characteristics of the two discharge types are plotted in Fig. 8.1 (L-type) and Fig. 8.2 (H-type). The only difference in the external controls is a slight change in the preprogrammed density during the ohmic phase. The line-averaged electron density $\bar{n}_e$ is $2.7 \times 10^{13} cm^{-3}$ during the ohmic phase of the L-type discharge and when it is raised to $3.1 \times 10^{13} cm^{-3}$ an H-type discharge occurs. Figure 8a shows $\bar{n}_e$ during the NI pulse

(hatched time interval) as it develops with density feedback control. In the case of an L-type discharge $\bar{n}_e$ tends to decrease. The H-type discharge starts like an L-type with decreasing density. But shortly after initiation of the NI pulse, $\bar{n}_e$ suddenly increases (as indicated by the dashed line) without modifications from the external controls. Figure 8b compares the central electron temperature T_e. Despite the higher density, T_e of the H-type discharge is higher by 350 eV. The improvement in electron energy content of the H-type discharge is obvious from a comparison of $(\beta_p + l_i/2)$ and β_{p1} as plotted in Fig. 8c. The increase in β_p due to NI in an H-discharge is nearly twice the increase in an L-type discharge.

4.1 The L-Type Discharge

In L-type discharges the plasma density generally decreases even with the gas flux ϕ_G from the external gas valve kept constant and in spite of the additional particles deposited within the plasma by the beam. An example of the time variation of the line average density $\bar{n}_e$ measured along a chord through the plasma center is plotted in Fig. 9. $\bar{n}_e$ decreases from $3.7 \times 10^{13} cm^{-3}$ during the ohmic phase to $2.4 \times 10^{13} cm^{-3}$ with neutral injection. ϕ_G is not regulated by a feedback system during the NI-pulse but is held constant at the level which maintained a density plateau in the ohmic phase. ϕ_G is about 3.5×10^{21} atoms/sec in the case shown in Fig. 9 with 1.2 MW injection power. The neutral source introduces $\phi_B \sim 3.1 \times 10^{20}$ fast atoms/sec and a negligible flux of cold atoms. When the beam is turned off (arrow 1 in Fig. 9), the density decreases even further before the density feedback system is activated again (at arrow 2) to restore the density to the original value.

The loss of plasma particles during neutral injection is particularly severe at medium plasma densities. At low density ($\bar{n}_e \sim 1 - 2 \times 10^{13} cm^{-3}$) the plasma density stays constant; at high density ($\bar{n}_e \sim 7 \times 10^{13} cm^{-3}$) the relative decrease in density with neutral injection is small: $\Delta \bar{n}_e / \bar{n}_e \sim 0.1$.

From the other tokamaks like ISX-B or DITE /11/, it is known that the plasma density during neutral injection could only be increased by strongly enhanced gas puffing from the outside. This phenomenon has been called "density clamping". The possibility that the density decrease is caused by a reduction of the recycling coefficient r or that it is, in case of ASDEX, a divertor related phenomenon will be briefly discussed, before we concentrate on the role of particle confinement during NI /12/.

4.1.1 Reduction in Recycling Coefficient and Refueling Efficiency, with NI

The actual plasma content at a given external gas flow Φ_G is determined by the effective particle confinement time τ_p^* which includes wall recycling. Owing to desorption and backscattering from the wall τ_p^* is much longer than the inherent particle confinement time τ_p. This pertains for limiter as well as divertor discharges. The difference in recycling between the two configurations is that in limiter discharges the immediate hydrogen exchange occurs between the plasma and the vessel wall, particularly the limiter /13/. In a divertor discharge the main recycling occurs between plasma and divertor chambers which are filled with hydrogen in the course of the discharge /14/. Hydrogen streams back from the divertor chambers and refuels the main plasma.

The particle content N of a divertor plasma is determined by the global particle confinement time τ_p of the plasma within the separatrix, the recycling coefficient r and the actual external gas flux $\gamma\Phi_G$ which fuels the plasma /14/:

$$N \cong \frac{\tau_p}{1-r} [\gamma\Phi_G + \Phi_B]$$

γ is the fueling efficiency which is experimentally found to be smaller than 1 for divertor plasmas /15/. Φ_B is the atom flux due to the NI-beams.

The reduction of one of the coefficients τ_p, r, or γ causes a decrease of the plasma content at constant external gas flow.

- A reduction of r can be expected during neutral injection. The ion temperature at the plasma edge, measured by a charge exchange analyzer, increases from typically 80 eV to 200 eV with neutral injection. From the increase in average energy of the ions and atoms hitting the wall, a reduction in recycling coefficient can be expected as the backscattered and the desorbed flux from the wall decrease, the latter because of a deeper hydrogen deposition within the wall. A decrease in r is manifested experimentally too. There are neutral injection cases in which the divertor plasma line density and the hydrogen pressure within the divertor chamber decrease together with the plasma content though the external gas flow is constant. Obviously the hydrogen content of the wall increases on account of the hydrogen content of plasma, boundary layer, and divertor. This can be described by a lower recycling coefficient.

- A further cause for the density decrease during neutral injection could be a reduction of the fueling efficiency, particularly as it is observed, that the electron temperature of the boundary layer increases with neutral injection. The increase in electron temperature may enhance the ionization processes within the boundary layer at the cost of dissociation processes. Thereby, the flux of Franck-Condon atoms into the main plasma may be reduced.

An increase of the external gas flux Φ_G by a factor of 3 during NI with 1.2 MW can reduce the amount of density decrease but it cannot prevent it. However, the enhanced gas flux sharply increases the boundary layer density as measured within the divertor chamber. Though the boundary layer density does not explicitly depend on the refueling efficiency, this behavior, particularly in comparison with the relatively moderate effect on the main plasma density, may imply a decrease of γ during neutral injection. Thereby the external gas flux and probably the recycling flux too, becomes less effective for refueling the main plasma.

4.1.2 Decrease of the Particle Confinement Time

Variation of the boundary layer density

Fig. 10a shows the decrease of the line density of the main plasma and Fig. 10b the variation of the boundary layer density measured in the divertor chamber during neutral injection. The main plasma line density is measured along three horizontal chords, one through the plasma center, one through z = a/2 and one through z = 3/4 a. (The insert to Fig. 10b is discussed in sec. 4.2.1).

The main plasma density decreases shortly after the beginning of the injection. The density along the outer chord (z = 3/4a) decreases 8.5 msec after the voltage to the injector source has been applied. The density along the middle chord (z = 1/2a) decreases after 13 msec. The density through the center seems to decrease even later, but there is no sharp discontinuity as in the other 2 cases. The initial phase of NI is accompanied by a peaking of the density profile.

A different behaviour is shown by the boundary layer density. It starts to increase 6 msec after the beginning of neutral injection. At that moment the hard X-ray radiation increases too, indicating that runaway electrons are lost from the plasma to the wall. The decrease in plasma density and the loss of runaway electrons is indicative of a loss of confinement. The deterioration of the confinement seems to start shortly after initiation of the beams first at the plasma edge from where it proceeds toward the plasma interior.

The variation of the boundary layer density supports the concept of a τ_p-reduction. The sudden increase in boundary layer density may originate from an enhanced particle efflux from the main plasma into the boundary layer till a new equilibrium is established.

The particle balance equation for the plasma within the separatrix in a divertor tokamak can be written /14/:

$$\frac{dN}{dt} + \frac{N}{\tau_p} = \gamma(\phi_G + \phi_D) \quad [+ \phi_B] \tag{1}$$

ϕ_D is the recycling flux from the divertor chambers. Within the short time scale of Fig., 10 the neutral pressure of the divertor chamber does not change so that ϕ_D is treated as a constant. With NI the atom flux ϕ_B from the beam has to be added.

The particle balance equation of the boundary layer plasma is written:

$$\frac{dn}{dt} + \frac{n}{\tau_{\shortparallel}^*} = (1-\gamma)\ (\phi_G + \phi_D) + \frac{N}{\tau_p} \tag{2}$$

n is the particle content of the boundary layer plasma, $\tau_{\shortparallel}^*$ is the effective confinement time of the boundary plasma given by the drift time from the main plasma to the neutralizer plate and incorporating the local recycling of the boundary layer plasma within the divertor.

The stationary solutions N_o and n_o of the equations (1) and (2) are:

$$\begin{aligned} N_o &= \tau_p \gamma\ (\phi_G + \phi_D)\ [\ + \tau_p \phi_B\ ] \\ n_o &= \tau_{\shortparallel}^*\ \ (\phi_G + \phi_D\ \ [+ \phi_B\ ]\ ) \end{aligned} \tag{3}$$

If we assume that at t = 0 the particle confinement time τ_p is reduced from τ_{p1} to τ_{p2}, and, for simplicity, neglect ϕ_B, then the plasma content decreases with time:

$$\frac{N\ (t)}{N_o} = \frac{\tau_{p2}}{\tau_{p1}} + \left(1 - \frac{\tau_{p2}}{\tau_{p1}}\right) e^{-t/\tau} \tag{4}$$

and decays to:

$$N = N_o\ \frac{\tau_{p2}}{\tau_{p1}} \tag{5}$$

The decay time τ_{eff} of the plasma content at t=0 is:

$$\tau_{eff} \equiv \frac{-N_o}{\frac{dN}{dt}\,(t=0)} = \frac{\tau_{p1}\tau_{p2}}{\tau_{p1}-\tau_{p2}} \qquad (6)$$

The time variation of the boundary layer content is:

$$\frac{n(t)}{n_o} = 1 - \gamma\,\frac{\tau_{p1}-\tau_{p2}}{\tau_{p2}-\tau_{\text{II}}^*}\,\left(e^{-t/\tau_{p2}} - e^{-t/\tau_{\text{II}}^*}\right) \qquad (7)$$

$\frac{n}{n_o}$ has a maximum at $t = t_M = \frac{\tau_{p1}\,\tau_{\text{II}}^*}{\tau_{p2}-\tau_{\text{II}}^*}\,\ell n\,\frac{\tau_{p1}}{\tau_{\text{II}}^*}$ (8)

At a line average density $\bar{n}_e = 3.7 \times 10^{13}\,cm^{-3}$ a particle confinement time τ_{p1} = 35 msec is assumed /14/. From eqs. (5) and (6) and the density as plotted in Fig. 10, τ_{p2} can be estimated. An average value τ_{p2} = 25 msec is used in the following. As the density profile peaks during the phase of decreasing confinement, the actual plasma outflux N/τ_{p2} may be higher than computed from the decrease of the line average density.

τ_{II}^* can be estimated from those cases with strong sawtooth oscillations during neutral injection. During a sawtooth relaxation, part of the plasma content is expelled into the boundary layer and transiently increases the density there. The decay of this density pulse occurs within approximately 10 msec which is identified with τ_{II}^* .

The dashed curves in Fig. 10a and b show the relative variation of the main plasma density and the boundary layer density calculated from eqs. (4) and (7) assuming γ = 0.4 /15/.

Though there are discrepancies in the exact description of the time varation of the two densities the occurence of a a maximum in the boundary density after the estimated time lapse and with the expected relative height supports the concept of reduced particle confinement. An exact description cannot be expected from this simplistic treatment (sudden decrease in τ_p and assuming $dN/dt \propto d\bar{n}_e/dt$) which

ignores effects caused by changes in recycling coefficient and refueling efficiency.

However, it can be ruled out that the peak in boundary layer density is caused by the outward displacement of the plasma column when the beam is switched on (see Fig.23). A simulation of the same shift, caused not by the beams but by a sudden decrease of the vertical field, showed no effect on the boundary layer density.

A peak in the boundary density as shown in Fig. 10b is observed during neutral injection into double null divertor discharges with constant external gas flux during injections and without strong sawtooth activity. Otherwise, the maximum in boundary layer density is masked by a sharp increase or by sawtooth fluctuations (inverted) in some cases with large amplitudes.

Measurements of the volume ionization rate

During the density plateau phase, the volume ionization rate

$$\int n_o n_e \langle \sigma v \rangle_i dV \qquad (9)$$

(n_o = neutral density, $\langle \sigma v \rangle_i$ = ionization rate coefficient) balances the ion efflux N/τ_p across the separatrix. In order to maintain a constant plasma content with a reduced confinement time, an enhanced ionization rate is required. The ionization rate is proportional to the H_α - D_α -radiation. (As the neutral injection experiments are generally carried out with H^o-beams fired into D^+-plasmas, sensors are used which measure the sum of H_α - and D_α -radiation.) In order to estimate the volume ionization rate, several H_α -monitors have to be placed around the torus. The H_α - D_α -intensity increases at all representative toroidal positions: At the injectors, owing to the ionization of beams and cold atoms from the source, at the location of gas input valve in case of a feedback-controlled discharge, but also at positions

between these distinguished points. From these observations, it can be concluded that the volume ionization rate increases. Nevertheless, the density decreases, confirming the hypothesis of a particle confinement time reduction during neutral injection.

Measurements of the hard X-ray radiation

In Fig. 11 the time variation of the line averaged plasma density $\bar{n}_e$, the plasma current I_p and the hard X-ray counting rate $\emptyset_x$ is plotted during 3 phases of the discharge - the build-up phase, the current and density plateau at the time of neutral injection (on an expanded time scale), and finally the termination of the discharge.

The decrease in density during neutral injection is accompanied by a sharp rise in the hard X-ray counting rate. It results from runaway electrons striking obstacles at the vessel wall (such as auxilliary limiters 10 cm away from the separatrix). As there is no further hard X-ray burst at the end of the discharge, as normally occurs, it is concluded that all runaway electrons are lost during neutral injection. The fluences of the hard X-ray radiation of a discharge with NI and the same type of discharge without NI are about the same. The hard X-ray radiation sets in shortly after the initiation of neutral injection at a time correlated with the decrease in plasma content. As in the case of the boundary layer density, it is experimentally checked that the radial expansion of the plasma column does not cause the sudden increase in hard X-ray flux.

The obvious decrease of the particle confinement time with neutral injection also affects the confinement of the runaway electrons. This sheds some light on the nature of the deterioration in confinement which could be caused by a partial ergodisation of the magnetic field lines (other mechanisms which simultaneously enhance cross-field transport of thermal and suprathermal particles, however, cannot be excluded).

We conclude, that the reduction of plasma density in L-type discharges is mostly due to a decrease in particle confinement time from about 35 msec during the ohmic phase to approximately 20-25 msec at P_{NI} = 1.2 MW. With rising power, we observe that the density decreases faster at the beginning of NI but it falls to a level which increases with beam power.

At high injection power, ϕ_B cannot be neglected. With $\phi_B \neq 0$, we find:

$$\frac{N}{N_o} = \frac{\tau_{p2}}{\tau_{p1}} \left(1 + \frac{\phi_B}{(\phi_G + \phi_D)}\right) \left(1 - e^{-t/\tau_{p2}}\right) + e^{-t/\tau_{p2}} \qquad (10)$$

The plasma content decays to:

$$N_\infty = N_o \frac{\tau_{p2}}{\tau_{p1}} \left(1 + \frac{\phi_B}{(\phi_G + \phi_D)}\right) \qquad (11)$$

and the decay time τ_{eff} is:

$$\tau_{eff} = \tau_{p2} \left(1 + \frac{N_\infty}{N_o}\right) \qquad (12)$$

The complications in determining reliable particle confinement times during NI have been mentioned above. In addition, at low P_{NI}, the actual rate of density decrease is masked by strong sawteeth on the measured density traces. Therefore, it is not possible, presently, to determine the precise variation of τ_p with P_{NI} (unlike τ_E^+ as shown in Fig. 5). From equ. (11) and (12) and the variation of the line density with increasing P_{NI}, we have to conclude that τ_p of L-type discharges further decreases with rising beam power.

4.1.3 Decrease of Energy Confinement Time

As with a material limiter, $\beta_p + \frac{l_i}{2}$ and β_{p^i} increase linearly with P_{NI}. For different plasma currents, $\Delta(\beta_p + \frac{l_i}{2})$ is plotted in Fig. 12 versus P_{NI}. Again, there is no saturation down to I_p = 200 kA. The current variation of β_p deviates from a I_p^{-2}- dependence.

Such a scaling would be expected from the lack of current dependence of τ_E of ohmic discharges and a largely current independent heating power. τ_E^+ of NI heated plasmas, however, increases with plasma current as already indicated in Fig. 5. The variation is roughly linear.

Figure 13 shows temperature profiles at an injection power of 1.25 MW and compares them to the profiles during the ohmic phase. In L-type discharges, all profiles are rather peaked. τ_E, calculated from these profiles, is 60 msec during ohmic heating and falls to 35 msec with NI.

The variation of the global energy confinement time with injection power is plotted in Fig. 18 for two different plasma currents. The decrease of τ_E with P_{NI} at low injection levels and then a leveling-off at high P_{NI} is similar to limiter discharges (see Fig. 5). Also as in limiter discharges, there is no density dependence of τ_E (documented by Fig. 20).

In summary, we can conclude that L-type discharges are characterized by simultaneously reduced particle and energy confinement times. The reduction is approximately by a factor 2.

4.2 The H-type Discharge

The deterioration of particle and energy confinement time is not an inevitable feature of NI heated tokamaks. As shown in Fig. 8, particle and energy content of H-type discharges suddenly increase at the transition from the L- into the H-phase.

4.2.1 Increase of Particle Confinement Time

The increase of density is mostly caused by an improvement in particle confinement and not by an enhanced impurity influx into the plasma. Figures 14a and b show experimental results to document this. Together with the line density, which is plotted for orientation, the bolometrically measured plasma radiation (Fig. 14b) and

the spectroscopically measured radiation of OVI and FeXVI are plotted versus time. All radiation signals are divided by the electron line density and plotted for the two discharge types (solid line: H-type; dashed line: L-type). During most of the injection phase the normalized impurity signals of H-type are lower than those of L-type discharges. (Without $\bar{n}_e$ -normalization, as it might be appropriate for the OVI-radiation, the oxygen-radiation is comparable in both cases.)

The improvement of particle confinement is effectively documented by the variation of density $\bar{n}_e$ in comparison to the external gasflux ϕ_G of density feedback controlled L- and H-type discharges. Figure 15 plots $\bar{n}_e$ and ϕ_G of two discharges, # 6028 L- and # 5991 H-type, during the NI pulse. In the L-type discharge, the reduction of density is counteracted by the gas valve which opens fully. Yet, the limited throughput cannot prevent the decay in particle content.

During the H-phase of shot # 5991, the density increases though the external gas valve closes and $\phi_G \sim 0$. The density increases above the ohmic level and decreases again after a maximum (causing the gas valve to open again). The NI pulse length is too short for establishing equilibrium again, which would give rise to the same density as during the ohmic phase, but at a lower value of ϕ_G than during the L-phase.

A global particle balance indicates (with limited accuracy as mentioned above) that τ_p during the H-phase resumes a value comparable to the one during ohmic heating. The extent of changes in refueling and recycling at the transition from L to H is difficult to estimate. As we observe an increase in electron and ion temperature at the plasma edge during the H-phase, a reduction both in γ and r is expected. A reduction of these two parameters would cause a decrease in plasma density (at constant ϕ_G) contrary to the observed variation.

Figure 16a shows the atom flux ϕ_a which emerges from the upper neutralizer plate (the experimental geometry is plotted as insert

to Fig. 16a). The atoms which give rise to ϕ_a are neutralized and backscattered ions which, according to their energy, originate in the main plasma and hardly in the cold boundary layer. At the transition L to H, ϕ_a decreases sharply to a level comparable to the one during the ohmic phase. The reduction in ϕ_a is the consequence of a corresponding reduction in ion outflux from the main plasma into the boundary layer due to the improvement in particle confinement. (The peaks in ϕ_a during the H-phase are caused by fluctuations in the edge plasma as discussed in Sec. 4.5).

On account of the lower particle fueling of the divertor chamber from the main plasma, the atom density rise there during the L-phase, is stopped. The atom density in the divertor chamber is constant or even decreasing during the H-phase. As a consequence, there is reduced particle backflow from the divertor chambers into the main plasma chamber for refueling the plasma.

This reduction in recycling flux is obvious from the H_α - D_α - radiation from the main plasma, or from the variation of the charge exchange flux ϕ_{cx} emitted from a zone close to the upper stagnation point. With the divertor configuration, the location of the recycling neutral density is around the stagnation points. ϕ_{cx} decreases at the transition L to H (see Fig. 16b), owing to a reduction in neutral density there and not to a decrease in ion density or temperature.

The density $\bar{n}_e$ increases in the H-phase despite the reduction in neutral density from external and recycling gas fluxes. In reversing the argument put forward in Sec. 4.1.2, the rise in density can only be achieved by an improvement in particle confinement and not by changes in boundary conditions or plasma wall interaction.

The sudden improvement in τ_p is also reflected by a corresponding change in boundary layer density. The insert to Fig. 10b shows its variation at the transition from the L- into the H-phase. The improvement in particle confinement gives rise to a temporary

reduction in ion outflux and, as a consequence, to a minimum in boundary layer density, causing the reversed variation as observed at the transition from the ohmic to the L-phase. Together with the confinement of thermal particles, the confinement of runaway electrons also improves at the transition into the H-phase. The hard X-ray flux decreases in the H-phase, nearly to its value during the ohmic phase.

4.2.2 Increase of Energy Confinement Time

As indicated in Fig. 8, the virtue of H-type in comparison to L-type discharges are higher β_p-values at the same injection power. Figure 17 shows $\Delta(\beta_p + l_i/2$ of H-type discharges at different plasma currents. For reference, the corresponding data of L-type discharges of Fig. 12 are replotted (dashed lines). Apart from the difference in absolute value of $\beta_p + l_i/2$, Fig. 17 also reveals that H-type discharges are only observed at $P_{NI} \geq 1.8$ MW.

So far, the highest β_p-value, measured at a plasma current of 200 kA (q=5.4), is 2.65 (the beam contribution to this value is ~0.3). This value corresponds to 65% of the aspect ratio A (A=4.1). The highest observed value of the volume averaged toroidal beta is $\langle\beta\rangle$ = 1.06% at q(a) = 2.8 (I_p = 380 kA).

Figure 18 plots the global energy confinement time of H-type discharges versus P_{NI} at 2 plasma currents and compares them with the values of L-type and ohmic discharges. The τ_E -values of Fig. 18 are deduced either from profile measurements or from β_p, and therefore they do not, or in case of τ_E^+, do negligibly include the beam energy.

The most important results of the investigations, presented here, are the high energy confinement times of H-discharges, which are comparable in magnitude to those of ohmic discharges. For H-type discharges, τ_E increases with plasma current. This current scaling of NI heated discharges is observed in L-type

discharges too and seems to be independent of the inherent confinement properties within the parameter range of our investigations. As ohmically heated discharges do not show a current variation in τ_E, the agreement in absolute value of τ_E between H-type and ohmic discharges is accidental.

In H-type discharges, we do observe a slight dependence of τ_E on plasma density, somewhat reminiscent of the ohmic phase. This density dependence, however, is only observable during a NI pulse with a moderate density variation. Figure 19 compares the rise in $\beta_p + \frac{l_i}{2}$ during NI of two discharges with different density variation. (The corresponding variation during a limiter discharge is plotted in Fig. 7). In one case (dotted line), the density decreases after a maximum; $\beta_p + l_i/2$ shows the same variation. In the other case (solid line), the density was kept constant by additional gas puffing and, as a consequence, $\beta_p + \frac{l_i}{2}$ stayed constant, too. In a wide density range and by plotting τ_E-values of different shots, this positive density variation of τ_E is lost within the scatter of the data points and no density variation is observed as shown in Fig. 20.

Characteristic of H-type discharges and possibly required for their formation are broad density and temperature profiles. An example is shown in Fig. 21. The dashed curve represents a semi-circular variation and serves as a guide to the eye for indicating the profile shape.

Figure 22a plots two density profiles obtained by Abel-inverting line densities, measured by HCN-laser and 2 mm µ-wave interferometry during a 380 kA discharge. The peaked profile is measured at the end of the L-phase just prior to the transition into the H-phase, the broad profile develops during the H-phase. Compared to the density profile of Fig. 21, measured at a plasma current of 300 kA, the density profile at higher plasma current seems to be even broader.

The broad profiles are caused by high densities and temperatures at the plasma edge. Figure 22b shows the rise of the ion temperature

at r = 35 cm from the L- into the H-phase and Fig. 22c compares the electron temperature at the same radial plasma position of an L and an H-type discharge. The latter measurements are carried out with a Thomson scattering system utilizing a 50 cps neodynium laser /16/. Five cm away from the separatrix, temperatures are about 1 keV.

4.3 Experimental Discrimination between L- and H-Type Discharges

There are several distinct differences between L- and H-type discharges which allow a clear classification. In Figs. 15 and 16, we have already pointed out the different recycling signals. In order to demonstrate the further differences in Fig. 23 we compare two subsequent discharges: # 4803 an L-type and # 4804 an H-type discharge. No change in the setting of the external discharge or NI parameters was carried out from the external control system between the two discharges.

The increase in β_p during the H-phase can immediately be seen from the variation of vertical field current and radial plasma position, the external constituents of the Shafranov relation. Figure 23a plots the vertical field current I_{VF} and Fig. 23b the radial plasma position $R-R_o$ of the two cases. As mentioned in Sec. 1, $\beta_p + \frac{l_i}{2}$ can be deduced from these values.

Because of the increased central electron temperature, but particularly on account of the T_e-profile broadening, the loop voltage U_l further decreases at the transition into the H-phase as documented by Fig. 23c. U_l is measured by two loops mounted within the vacuum vessel close to the plasma surface. The two loops are installed in such a way that the voltage, induced by the vertical field variation, is largely compensated. U_l-values close to zero are observed.

There is also a pronounced increase in fusion neutron flux ϕ_n from the plasma at the transition L to H as plotted in Fig. 23d. The flux increase is partly caused by the increase in density

and the profile broadening. Neutron spectra, obtained from the exposure of nuclear emulsion plates /17/ indicate non-thermal contributions to the neutron production rate at high NI powers. These non-thermal contributions seem to be higher in H- than in L-discharges.

4.4 Operational Regime of H-Discharges

In the following, the experimental conditions and the range of plasma parameters which allow the development of the H-regime are described[x]. Figure 17 reveals that there are only L-type discharges at an injection power level $P_{NI} \leq 1.8$ MW. Above this power level, both discharge types are encountered depending on $\bar{n}_e$ and B_T. Figure 20 indicates that the H-phase develops above $\bar{n}_e = 3 \times 10^{13} cm^{-3}$ at $I_p = 300$ kA. The high density values are achieved by strong gas puffing during the NI pulse. Under these circumstances, density and recycling signals increase sharply and it is, in some cases, difficult to define the discharge type. At high density, L-type discharges can develop again, possibly because of the limitation in available injection power or beam penetration. H-type discharges have been obtained at plasma currents between 200 and 450 kA. A decrease of the toroidal magnetic field resulting in a lower $q(a)$-value can lead to a transition into the L-regime. H-type discharges have not been observed for cylindrical values of $q(a) < 2.45$.

The H-regime is characteristic of divertor discharges in ASDEX. It has never been obtained in ASDEX limiter discharges. τ_E^+-values of toroidal limiter discharges plotted in Fig. 5 are comparable to those of L-type discharges (see Fig. 18). Given a limited number of shots with material limiters, the accuracy of this statement is also based on the observation that the H-regime disappears at the transition from divertor to limiter discharges. In sequential discharges, both divertor and limiter behaviour could be compared.

---

[x] The limited material presented at the workshop, allowed the conclusion that a further premise for the development of the H-regime is deuterium as working gas. Meanwhile, the H-regime has been explored in hydrogen, too. These results will be published elsewhere.

The H-type characteristics of the divertor discharges with NI always disappeared in the limiter discharge, which followed. A limiter-separatrix distance of 2 cm, which corresponds to the density fall-off length in the boundary layer, is sufficient for the deterioration.

The observation that the H-type does not develop in limiter discharges may be the result of the higher impurity content of these discharges. The role of impurities in the formation of the H-type discharges was empirically studied by puffing in small amounts of low-Z (CH_4) and high-Z (Kr) gases into the discharges. The addition of impurities deteriorates an H-type discharge or prevents its formation. A premise for the attainment of the H-regime seems to be the development of broad temperature profiles, which are compatible with the divertor configuration with its lack of additional edge cooling, and where high edge temperatures do not lead to an intolerable impurity inflow. Radiation, particularly from the plasma edge due to added impurities or those released from the limiter, may - in case of ASDEX - suppress the formation of broad profiles and prevent the attainment of the H-regime.

4.5 MHD-Observations

The attainment of H-type discharges with the improved confinement properties is independent of the presence of sawteeth oscillations during the ohmic phase. However, it is generally easier to maintain a stable OH-discharge with sawteeth present. Fig. 24a shows the variation of the central line density due to sawteeth during the ohmic phase and with NI at different numbers of sources. All cases shown in Fig. 24a are L-type discharges. The different density traces are shifted vertically for discrimination. During the ohmic phase, the line density values are identical for all discharges. A sawtooth causes a sudden reduction in line density because of a broadening of the density profiles and also a loss of particles. The sawteeth in the density as plotted in Fig. 24a coincide with sawteeth in the electron temperature measured by ECE.

The sawtooth repetition time $\tau_{s.t.}$ increases with beam power and, at a beam power above 2 MW (7 sources), there is a single sawtooth shortly after beginning of NI but no one more during the NI pulse. Figure 24b compares $\tau_{s.t.}$ of limiter and divertor discharges. Sawteeth are observed in limiter discharges up to the highest injection power. For $P_{NI} > 1$ MW, the sawtooth period is roughly constant around 30 msec.

Though the power limit of ~2 MW for sawtooth-free injection into divertor discharges seems to coincide with the power limit for the attainment of H-type discharges, above this power level, L-type as well as H-type discharges are free of sawteeth. The sawtooth-free NI-phase seems to be more a characteristic of divertor discharges.

In H-type discharges, the plasma center is sawtooth-free but relaxation phenomena occur which affect the outer plasma region between r = a/2 and a. A burst is detected as a high frequency (80-120kHz), low amplitude oscillation by Mirnov coils and as a heavily damped low frequency (~6kHz) oscillation with high amplitude by those soft X-ray diodes which view the outer plasma zones.

These bursts lead to periodic density and temperature reductions between a/2 and a. In the plasma center, the gross plasma parameters remain unaffected. These features are documented in Fig. 25a which shows the variation of the electron temperature (ECE) in the center and near the plasma edge from the ohmic into the NI phase. Figure 25a exemplifies the transition from the ohmic sawtooth discharges, with the sawteeth affecting the plasma center, into the H-phase during NI, with bursts affecting the outer plasma layers. Figure 25b shows the effect of a single burst in a better time resolution to indicate more clearly its consequence on the electron temperature. Further plotted is the reduction in line density and, as a result of the β_p-loss by a burst, the inward displacement of the plasma. The edge location of these fluctuations is also indicated by impurity line radiation. OVI-radiation is modulated by bursts because it originates from the plasma periphery, while FeXVI-radiation from the plasma center is unaffected (see Fig. 14b).

Because of the particle loss and the sudden increase in fall-off length of the boundary layer density, the plasma-wall interaction is intensified during a burst which is obvious from all recycling signals (e.g.see Fig. 16) but can also be seen in high speed films taken during the NI pulse.

The repetition time of these bursts can vary in a wide range from 0.3 msec up to 60 msec. As each burst gives rise to a slight reduction in β_p, their erratic nature causes the high scatter in the τ_E-values of Fig. 18.

We observe, that bursts affect the thermal plasma. There are no indications that they also influence the high energy beam ions. The observed thermal particle losses are isotropic.

4.6 Beam Deposition in H- and L-Discharges

An alternative explanation to the changed confinement properties between L- and H-discharges is a loss of injection power to the wall in L-type discharges and therefore a degraded performance of this discharge type. The question of particle and energy depositions is generally addressed by measuring the charge exchange efflux of the injected species, favorably near the injection angle. Tangential charge exchange measurements up to the injection energy have not yet been carried out on ASDEX. In the perpendicular direction, the hydrogen charge exchange flux can be measured up to 32 keV before the signal disappears in the background. From these measurements, no significant differences between L- and H-type discharges have been observed.

The main argument against the possibility of different energy deposition is drawn from the radial inward displacement of the plasma as soon as the beams are switched off (see Fig. 23b). Figure 26 plots the amplitude of this excursion versus beam power P_{NI}. There is a linear relationship between the two, and the absolute values of ΔR for L- and H-discharges are the same in the power range where H-discharges are possible. The amplitude

of the inward movement, however, is the result of a complicated interplay between fast particle energy content, response of the vertical field feedback system and possibly eddy-currents in the vessel. Nevertheless, the agreement in ΔR of L- and H-discharges should rule out that half of the beam power is lost in the case of an L-discharge, as would be necessary to explain the different energy content to an H-discharge at the same confinement time.

4.7 Role of Electron Transport in Energy Confinement

Transport code analysis shows that the deterioration in energy confinement is caused by an enhanced electron transport /9/. The limitation in heating efficiency of a NI heated plasma due to the electron losses is documented by the variation of the central electron temperature with beam power, as plotted in Fig. 27. The results of Fig. 27a are obtained from L- and H-type deuterium discharges. Those plotted in Fig. 27b are restricted to L-type hydrogen discharges. Common to all L-type discharges shown in Fig. 27 is a rise in $T_e(0)$ with injection power up to a saturation level. The saturation level increases with toroidal field B_T and plasma current I_p . The increase caused by B_T (or $q(a)$) is due to a peaking of the T_e-profile. There is no indication of a dependence of the plasma energy content on toroidal field (B_T-scans, however, have not yet been carried out in a wide range). The increase in slope and saturation level of $T_e(0)$ with current, as shown in Fig. 27b, is one reason for the plasma current scaling of the energy confinement time.

Though the central T_e-values become invariant, the loop voltage still decreases with increasing beam power indicating a further increase in plasma conductance. This is caused by a broadening of the T_e-profile toward higher beam power which also causes a broadening of the current density profile (and a reduction of l_i as noted in Sec. 2).

In H-type discharges (open symbols in Fig. 27a), no saturation in $T_e(0)$ is observed stressing again the role of electron transport for global energy confinement. Because of the higher density

in the H-regime, the H-type data points correspond to lower values of $P_{abs}/\bar{n}_e$.

From the linear point part of $T_e(0)$ vs. $P_{abs}/\bar{n}_e$ an electron heating efficiency $\eta_e \equiv \bar{n}_e \Delta T_e(0)/P_{abs}$ can be defined[x]. The highest observed value of H-type discharge is $\eta_e = 2.3 \times 10^{13}$ $(eVcm^{-3}kW^{-1})$. Because of the saturation in $T_e(0)$, η_e is of restricted importance in case of L-type discharges and cannot be used for any scaling.

4.8 Ion Heating Efficiency

In Fig. 28 the central ion temperature $T_i(0)$ is plotted versus the absorbed power normalized against the density for I_p = 300 kA and 380 kA. The heating efficiency η_i ($\eta_i \equiv \Delta T_i \bar{n}_e/P_{abs}$) for L-type discharges is between (1.6-2.8) x 10^{13} eV cm^{-3} kW^{-1}; for H-type discharges, it is between (2.5-4.2) x 10^{13} eV $cm^{-3}kW^{-1}$, and η_i is observed to increase with plasma current. It seems likely on the basis of the power transferred from the ions to the electrons, that the higher heating efficiency of H-type discharges is the response of the ions to the increased electron temperature.

---

[x] The definition of $\eta_e = \Delta T_e/P_{abs}$ is appropriate on the basis of the Alcator scaling with $\tau_E \alpha n_e$. Under these circumstances, ΔT_e is independent of $\bar{n}_e$. As we find τ_E independent of $\bar{n}_e$, we adopt the definition of η_e as stated above.

Summary

NI has been carried out into material limiter and divertor discharges of ASDEX. With NI into divertor discharges two operational regimes, one with high β_p (H-type) and one with low β_p (L-type), are observed. Hydrogen and deuterium have been used as working gas.

As in the ohmic case, the confinement properties of NI heated deuterium plasmas ($H^o \rightarrow D^+$) are superior to those of hydrogen plasmas ($H^o \rightarrow H^+$).

In all cases investigated, a linear increase in β_p with injection power P_{NI} has been observed up to the highest values of P_{NI} (3.1 MW) and down to the lowest plasma current (200 kA). The highest β_p-value, measured at I_p = 200 kA of an H-type discharge is 2.65, which is 65 % of the aspect ratio.

The global energy confinement time τ_E of limiter and L-type divertor discharges is found to deteriorate with NI. An injection power which is about twice the power input during the ohmic phase is sufficient to reduce τ_E to half the ohmic value. A further increase of P_{NI} causes only a moderate further drop of τ_E. In L-type divertor discharges a reduction in particle confinement time τ_p is observed simultaneous to the deterioration of energy confinement. Like τ_E, τ_p is found to decrease also by about a factor of 2. The conclusions drawn with respect to the particle confinement, require experimental conditions with controlled plasma wall contact. These requirements are established in divertor discharges, but the results and conclusions seem also to be relevant for limiter discharges with density clamping. The consequences of NI have also a detrimental effect on the containment of run-away electrons, an observation, which might indicate partial magnetic field ergodization as loss channel.

H-type divertor discharges start with L-type characteristics but, shortly after beginning of NI, they go into another phase with improved energy confinement time. Together with τ_E

an improvement of the particle confinement time is observed too. The absolute values of τ_E and τ_p are comparable to those of ohmic discharges. This agreement, however, is accidental because the density- and plasma current scaling of ohmically heated discharges differ from those during NI. In L- and H-type discharges, an increase in τ_E with I_p is observed. In L-type discharges, there is no increase in τ_E with $\bar{n}_e$ as in ohmic discharges; in H-type discharges, a weak density response of τ_E has been noted.

The deterioration and improvement of energy confinement seem to be corollary to changes in electron confinement. In L-type divertor discharges, saturation in the central electron temperature with beam power is observed. The saturation level, however, increases with plasma current. No such saturation has yet been observed for H-discharges.

The observation of restored energy confinement may indicate that the generally observed degradation in confinement with NI is not an unavoidable consequence of NI as a heating method, nor a general property of high temperature, or of high β_p plasmas.

The new regime extends over a wide range of q-values, plasma currents and densities, although, thus far, it has only been obtained in divertor discharges. A prerequisite for its formation seems to be the development of broad temperature profiles, which are compatible with the divertor configuration with its lack of additional edge cooling, and where high edge temperatures do not lead to an intolerable impurity inflow. A broad current density profile is indicated by a lack of sawtooth activity in the plasma center. Although a sawtooth-free discharge may not be sufficient in itself to develop the H-regime, the resulting broad pressure and current density profiles may represent the necessary criterion for its formation.

Acknowledgements

We wish to express our appreciation to the ASDEX and Neutral Injection operational teams for their efforts. Thanks are due to H. Volkenandt, B. Meider and I. Hermann for preparing the manuscript and to E. Meservey for critically reading it.

References

/1/ Keilhacker, M., et al., Proc. 8th Int. Conf. on Plasma Physics and Contr. Nucl. Fusion Research, Brussels, 1980, Vol. II, IAEA, Vienna (1981) 351.

/2/ Stäbler, A., et al., 9th Symp. on Eng. Problems of Fusion Research, Chicago (1981) 767.

/3/ Lister, G.G., et al., Proc. 3rd Symp. on Heating in Toroidal Plasmas, Varenna (1976) 303.

/4/ Gernhardt, J., et al., "Design and Electronic Compensation of a Diamagnetic Loop and its Application on the ASDEX Tokamak", IPP-Report III/84 (1983).

/5/ Murakami, M., et al., Proc. 7th Int. Conf. on Plasma Phys. and Contr. Nucl. Fusion Research, Innsbruck, 1978, Vol. I, IAEA, Vienna (1979) 269.

/6/ Lomas, P.J., et al., Proc. 10th Europ. Conf. on Contr. Fusion and Plasma Physics, Moscow, 1981, A1.

/7/ Vernickel, H., et al., Jour. Nucl. Mat. Vol. 111&112 (1982) 317.

/8/ Gaudreau, M., et al., Phys. Rev. Letters 39 (1977) 1266.

Klüber, O. and Murmann, H., "Energy Confinement in the Tokamak Devices Pulsator and ASDEX", IPP-Report III/72, Garching (1982).

/9/ Becker, G., et al., Nucl. Fusion 22 (1982) 1589

/10/ Wagner, F., et al., Proc. 3rd Joint Varenna Grenoble Intern. Symp., Varenna 1982, Vol. I, CEC, Brussels (1982) p. 35.
Wagner, F. et al., Phys. Rev. Letters 49 (1982) 1408.
Wagner, F. et al., Proc. 9th Int. Conf. on Plasma Physics and Contr. Nucl. Fusion Research, Baltimore, 1982, paper IAEA-CN-41/A-3.

/11/ Swain, D., et al., Proc. 9th Europ. Conf. on Contr. Fusion and Plasma Phys., Oxford (1979) paper B2.2.
Axon, K.B., et al., Proc. 8th Int. Conf. on Plasma Physics and Contr. Nucl. Fus. Research, Vol. 1, IAEA, Vienna (1981) p. 413.

/12/ Wagner, F., et al., "Variation of the Particle Confinement during Neutral Injection into ASDEX Divertor Plasmas", IPP-Report III/78, Garching (1982).

/13/ Wagner, F., "Investigation of Limiter Recycling in the Divertor Tokamak ASDEX", IPP-Report III/71, Garching (1981).

/14/ ASDEX-Team, presented by Wagner, F., Proc. of IAEA Techn. Committee Meeting on Divertors and Impurity Control, edited by M. Keilhacker and U. Daybelge, Max-Planck-Institut, Garching (1981) p. 40.

/15/ Mayer, H.M., et al., Jour. Nucl. Mat. Vol. 111&112 (1982 204.

/16/ Röhr, H., et al., Nucl. Fusion 22 (1982) 1099.

/17/ Hübner, K., Steinmetz, K., to be published.

Figure Captions

Fig.1: Central electron (measured by electron cyclotron emission) and ion (measured by passive charge exchange) temperature during neutral injection (NI). The NI phase is marked, as in the following plots, by a hatched area.

Fig.2: Variation of $\beta_{p\perp}$ (measured by a diamagnetic loop) and the global energy confinement time τ_E^+, deduced from it, at the change-over from hydrogen to deuterium as working gas in ohmic discharges.

Fig.3: Increase in $(\beta_p + \frac{l_i}{2})$ with respect to the ohmic phase versus the power P_{NI} injected into the vessel for toroidal and poloidal limiter and divertor discharges with hydrogen ($H^o \rightarrow H^+$) and deuterium ($H^o \rightarrow D^+$) target plasmas and at different plasma currents.

Fig.4: The two limiter configurations are sketched (poloidal cross-section) together with the limiter compatible divertor configurations (dashed contours).

Fig.5: τ_E^+ of limiter discharges versus P_{NI} with hydrogen and deuterium as working gas and at different plasma currents

Fig.6: τ_E(●,O), deduced from plasma profiles, and τ_E^+(■,□) versus line average plasma density $\bar{n}_e$ of ohmic (I_p = 250 - 300 kA) and NI heated plasmas.

Fig.7: Variation of $\beta_p + \frac{l_i}{2}$ during NI into a toroidal limiter discharge with rising density.

Fig.8: Time dependence of various plasma parameters of L-type (Fig. 8.1) and H-type (Fig. 8.2) discharges: a) line-averaged density $\bar{n}_e$, b) electron temperature T_e (no signal during the dotted intervals because of an offset check), c) $(\beta_p + l_i/2)$ from plasma equilibrium and $\beta_{p\perp}$.
The dashed vertical line indicates the transition from the L- to the H-regime, P_{NI} = 2.42 MW.

Fig.9: Time dependence of $\bar{n}_e$ during the NI pulse which is terminated at arrow 1. At arrow 2 the density feedback system is activated to restore the original density.

Fig.10 a): Line density versus time measured along three horizontal chords with different distances (Z) from the plasma center.

b): Line density of the boundary plasma measured in the divertor chamber.

Insert: Variation of the boundary density at the transition from the L- to the H-phase.

The dashed curves are the calculated quantities as described in the text.

Fig.11: Plotted are plasma current I_p, line average density $\bar{n}_e$ (z=0) and hard X-ray flux ϕ_x through three phases of the discharge: The initial phase, the neutral injection phase with expanded time scale, and the termination of the discharge.

Fig.12: Increase in $(\beta_p + \frac{l_i}{2})$ for various plasma currents for L-type discharges.

Fig.13: Electron and ion temperature profiles of L-type discharges in comparison to profiles during the ohmic phase.

Fig.14: a) Plasma radiation from an L- and an H-type discharge as measured by a bolometer. The signal is divided by the plasma density. The line average density is replotted for reference.

b) Radiation of OVI and FeXVI each normalized against plasma density from the two discharge types.

The arrows indicate the transition from the L- into the H-phase.

Fig.15: Time dependence of line averaged density $\bar{n}_e$ and external gas flux Φ_G of L-type (left column) and H-type (right column) discharges. The dashed line indicates the transition from the L- into the H-regime.

Fig.16: Time dependence of the atom flux Φ_a which emerges from the neutralizer plate and the charge exchange flux Φ_{cx} emitted near the stagnation point during NI, and at the transition L to H (indicated by the vertical line).
Insert: Notifies the origin of the two fluxes Φ_a and Φ_{cx}.

Fig.17: Increase in $(\beta_p + l_i/2)$ for various plasma currents for H-type discharges. The values of L-type discharges (Fig.12) are replotted for reference (dashed lines).

Fig.18: Thermally (τ_E, plotted as crosses) and magnetically (τ_E^+, plotted as circles) measured confinement times for two plasma currents and for L-type and H-type discharges. The range of τ_E of ohmic discharges is indicated by error bars for hydrogen (H^+) and deuterium (D^+) plasmas.

Fig.19: Time dependence of $(\beta_p + \frac{l_i}{2})$ during NI into two discharges with different density variation during the H-phase. The transition into the H-phase is indicated by arrows.

Fig.20: Global energy confinement time versus density for L- (solid symbols) and H-type (open symbols) divertor discharges (τ_E: +, x, τ_E^+: other symbols). In case of the triangles, no clear assignment of the discharge type has been possible. The dashed lines separate the data points obtained at different plasma currents.

Fig.21: Temperature and density profiles during an H-type discharge. The dashed arcs indicate a semi-circular variation and are plotted to point out the profile shape.

Fig.22 a) Density profiles obtained from Abel-inverted HCN-laser and 2 mm μ-wave interferometer data. The L-type profile is measured just prior to the transition into the H-phase.

b) Variation of the charge exchange ion temperature at the transition from the L- into the H-phase at $r = 7/8\ a\ (35\ cm)$.

c) Comparison of the electron temperature at the same radial position of an L- and an H-type discharge. The measurements are carried out with a 50 cps Thomson scattering system.

Fig.23: Comparison of several plasma parameters of an L- (#4804, dashed curve) and an H-type discharge (#4804, solid curve)
a) vertical field current I_{VF} b) shift of the plasma position $R-R_o$ (R_o = 165 cm) c) loop voltage U_L
d) neutron count rate ϕ_n.
The transition into the H-phase is indicated by arrows.

Fig.24: a) Variation of the line averaged density indicating sawteeth during NI with different numbers of NI sources. The density traces are shifted vertically for clarity. The densities during the ohmic phase agree in all cases.

b) Sawtooth repetition time $\tau_{s.t.}$ versus beam power for limiter and divertor discharges. The NI pulse length is 200 msec as indicated.

Fig.25: a) Variation of the central (r=1 cm) and peripheral (r=30 cm) electron temperature. Demonstrated is the transition from the ohmic phase with sawteeth into the H-phase with bursts. (No signal during the minima because of an offset check.)

b) Shown is the effect of bursts on line averaged density $\bar{n}_e$, on radial plasma position $R-R_o$ and electron temperature in an expanded time scale.

Fig.26: Radial excursion ΔR of the plasma column when the NI beams are switched off versus P_{NI} for L- and H-type discharges.

Fig.27: Variation of the central electron temperature versus absorbed beam power P_{abs} normalized against density $\bar{n}_e$:
a) comparison between L- and H-type discharges at different toroidal field values with NI into deuterium plasmas.
b) at different plasma currents with NI into hydrogen discharges.

η_e is the electron heating efficiency.

Fig.28: Central ion temperature versus $P_{abs}/\bar{n}_e$ for L- and H-type discharges at different plasma currents.
η_i is the ion heating efficiency.

Fig. 1

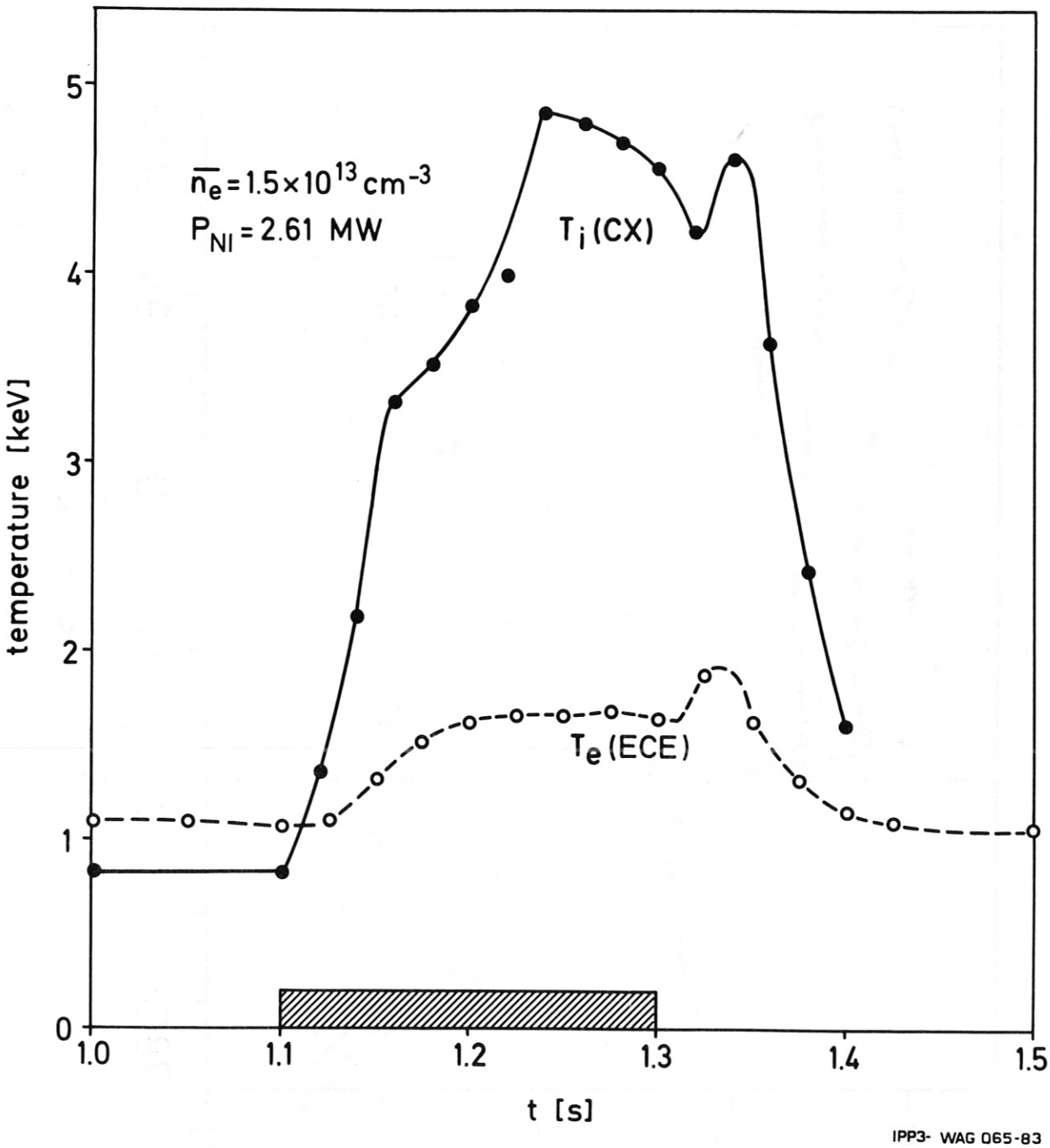

IPP3- WAG 065-83

Fig. 2

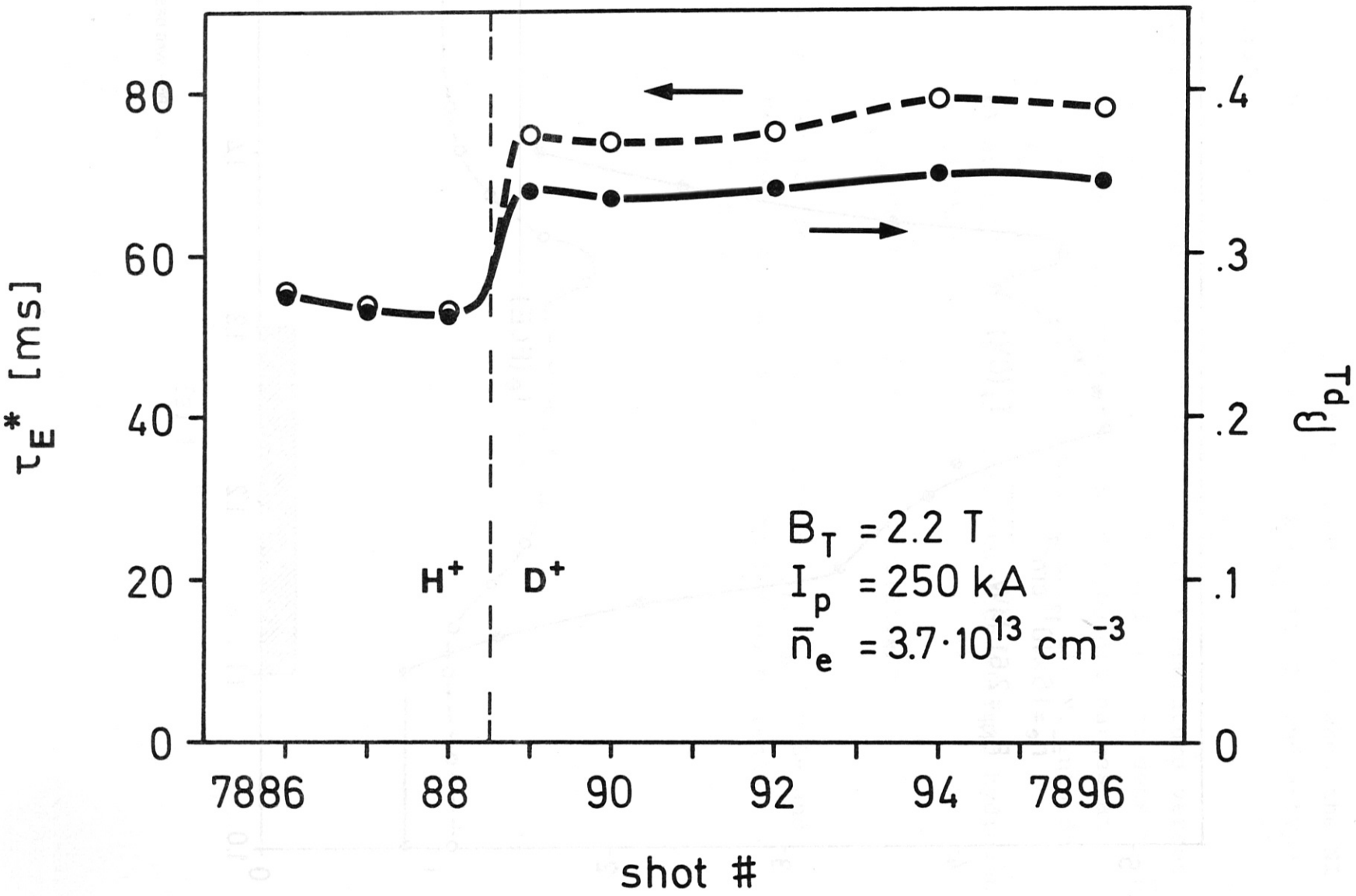

IPP3- WAG 066-83

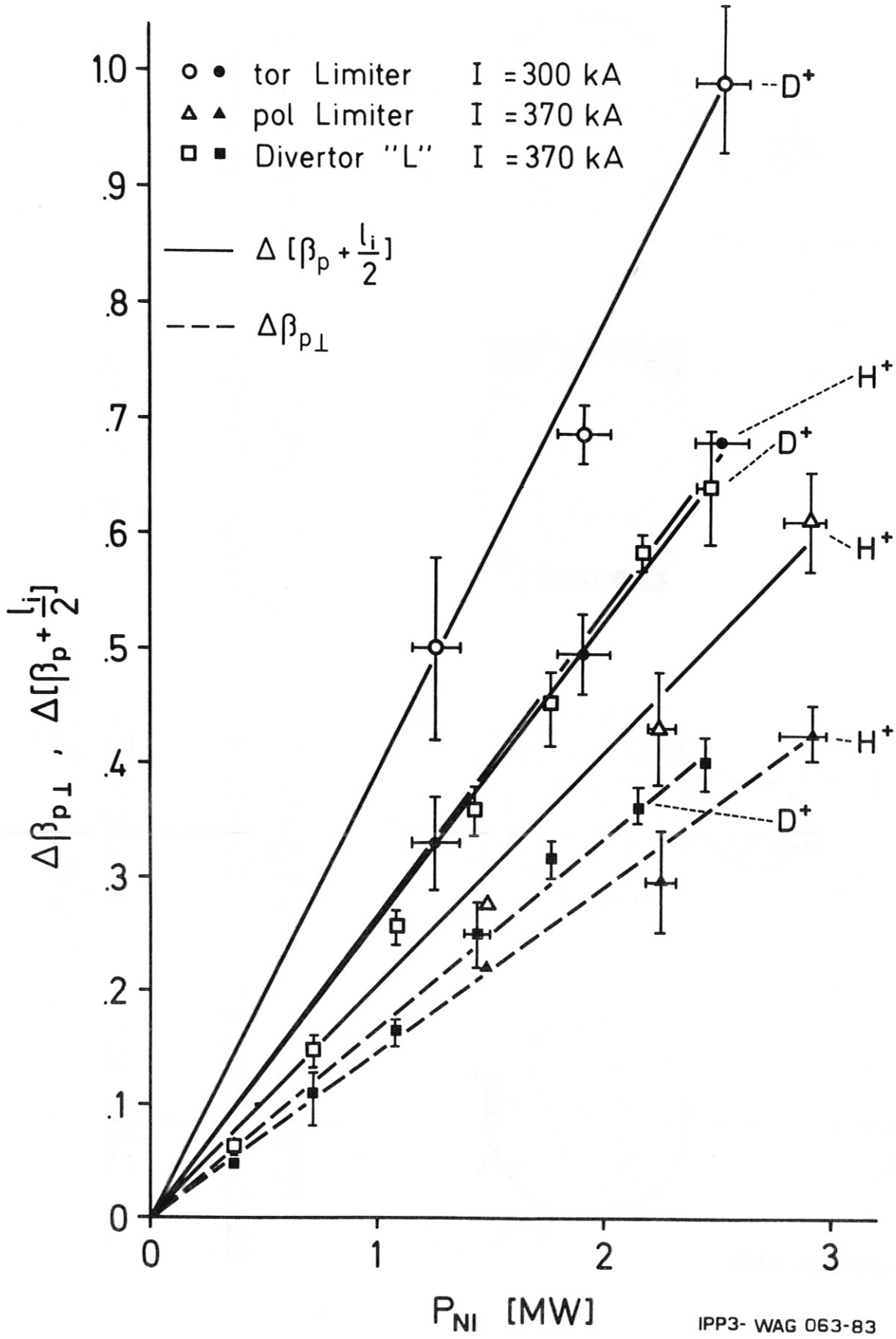
tor Limiter I = 300 kA
pol Limiter I = 370 kA
Divertor "L" I = 370 kA
$\Delta\left[\beta_p + \frac{l_i}{2}\right]$
$\Delta\beta_{p\perp}$
D+
H+
D+
H+
H+
D+
1.0
.9
.8
.7
.6
.5
.4
.3
.2
.1
0
0
1
2
3
$\Delta\beta_{p\perp}$, $\Delta\left[\beta_p + \frac{l_i}{2}\right]$
P_{NI} [MW]
IPP3- WAG 063-83

Fig. 3

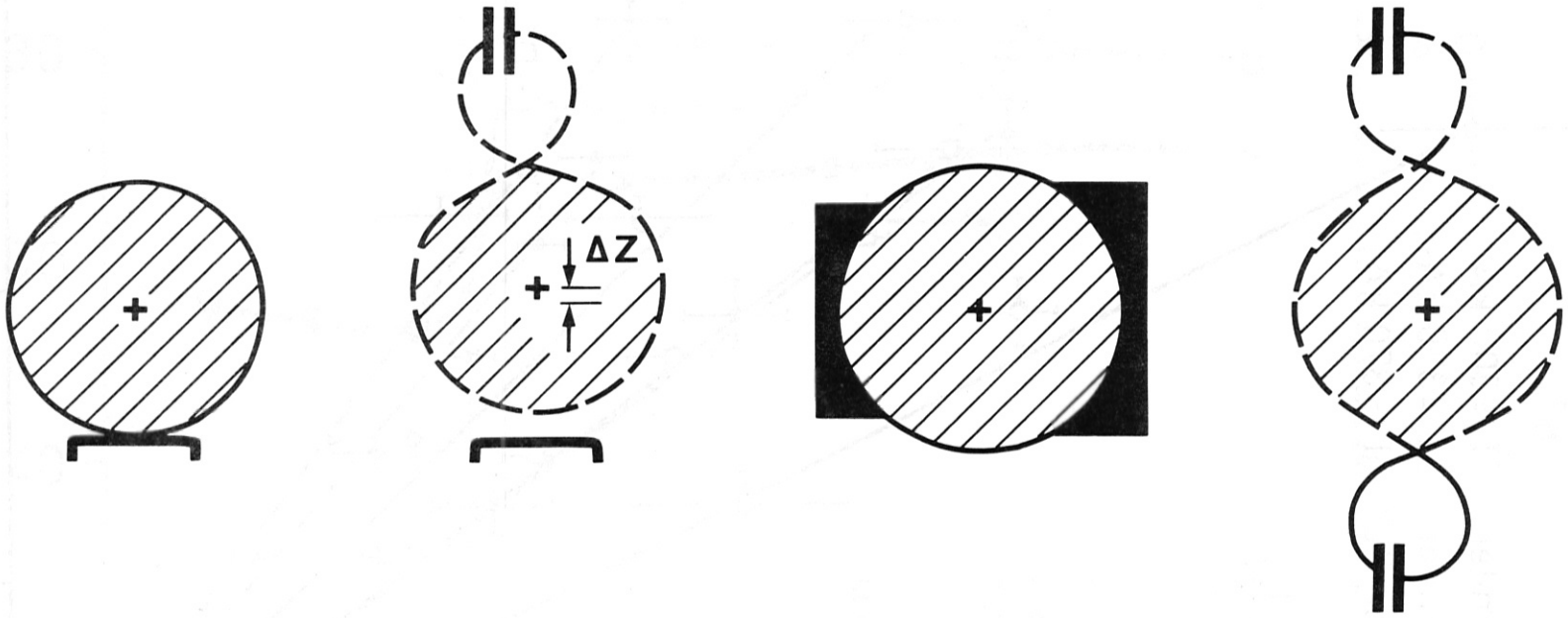

toroidal carbon limiter	single - null divertor	poloidal carbon limiter	double - null divertor
a = 38.5 cm	a = a(ΔZ) typically 36 cm	a = 40 cm	a = 40 cm

IPP3- WAG 064-83

Fig. 4

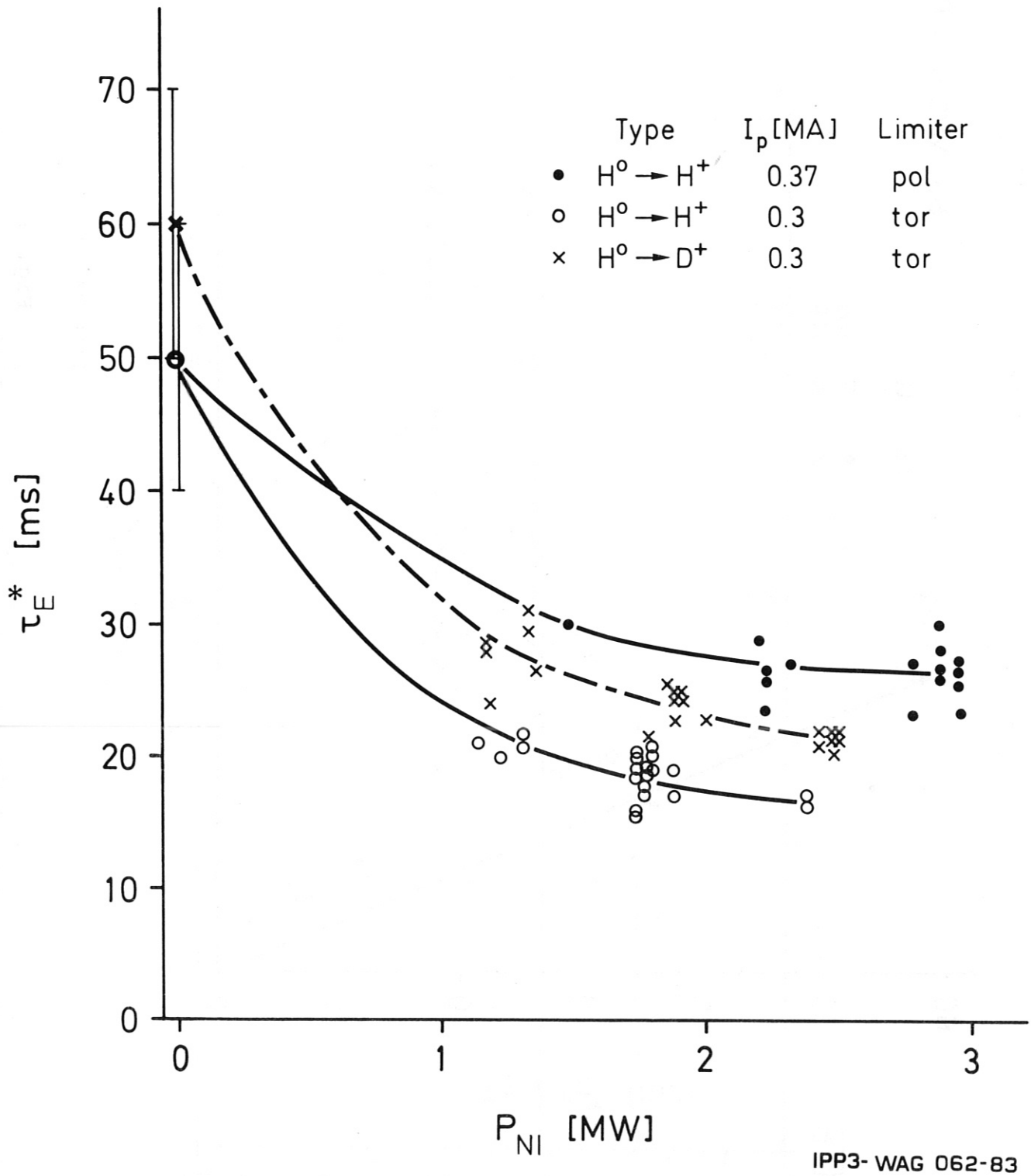
Type
I_p [MA]
Limiter
• $H^o \rightarrow H^+$ 0.37 pol
o $H^o \rightarrow H^+$ 0.3 tor
× $H^o \rightarrow D^+$ 0.3 tor
τ_E^* [ms]
P_{NI} [MW]
0
10
20
30
40
50
60
70
0
1
2
3
IPP3- WAG 062-83

Fig. 5

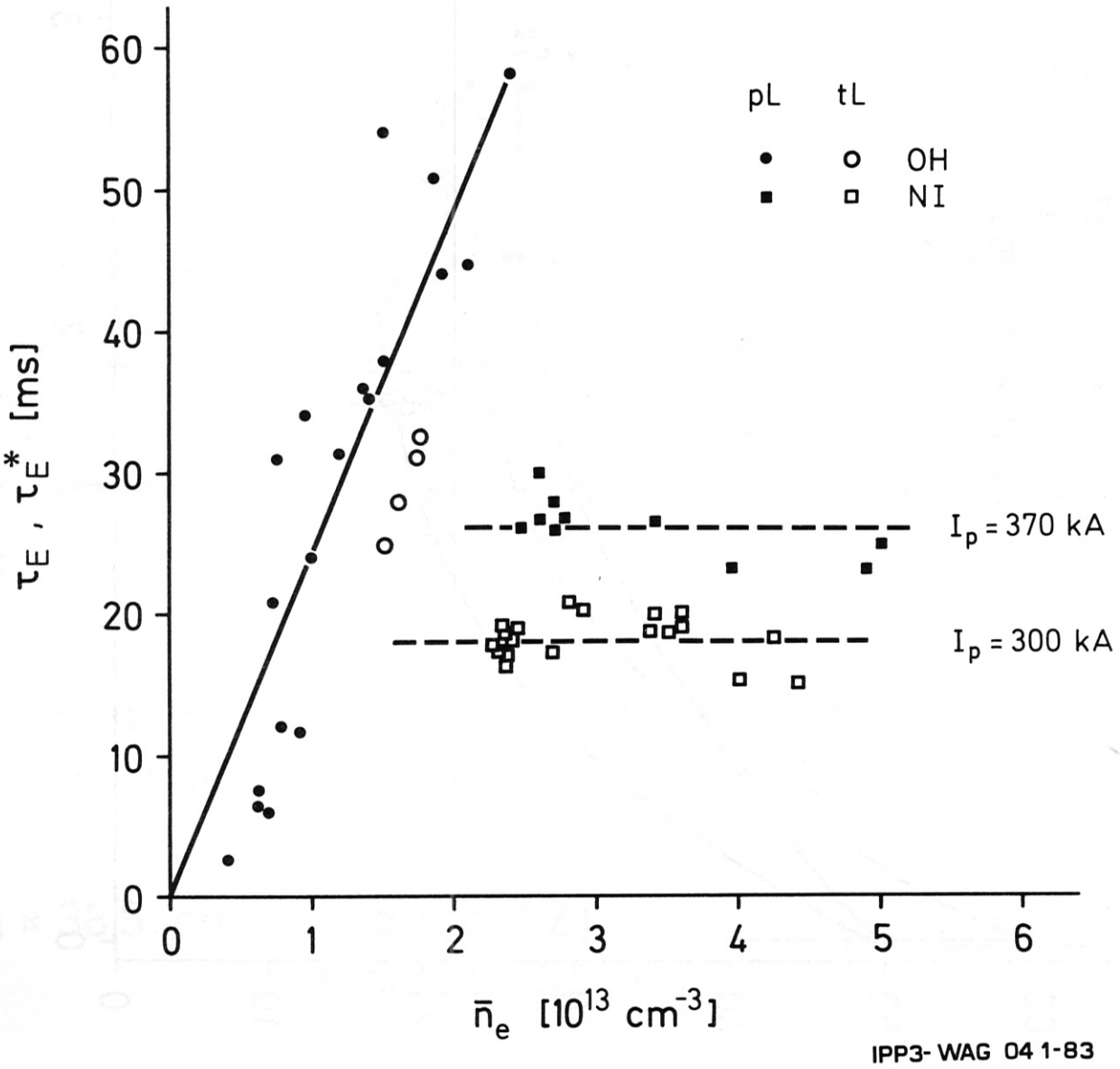
60
50
40
30
20
10
0
0
1
2
3
4
5
6
τ_E , τ_E^* [ms]
$\bar{n}_e$ [10^{13} cm^{-3}]
pL tL
OH
NI
I_p = 370 kA
I_p = 300 kA
IPP3- WAG 04 1-83

Fig. 6

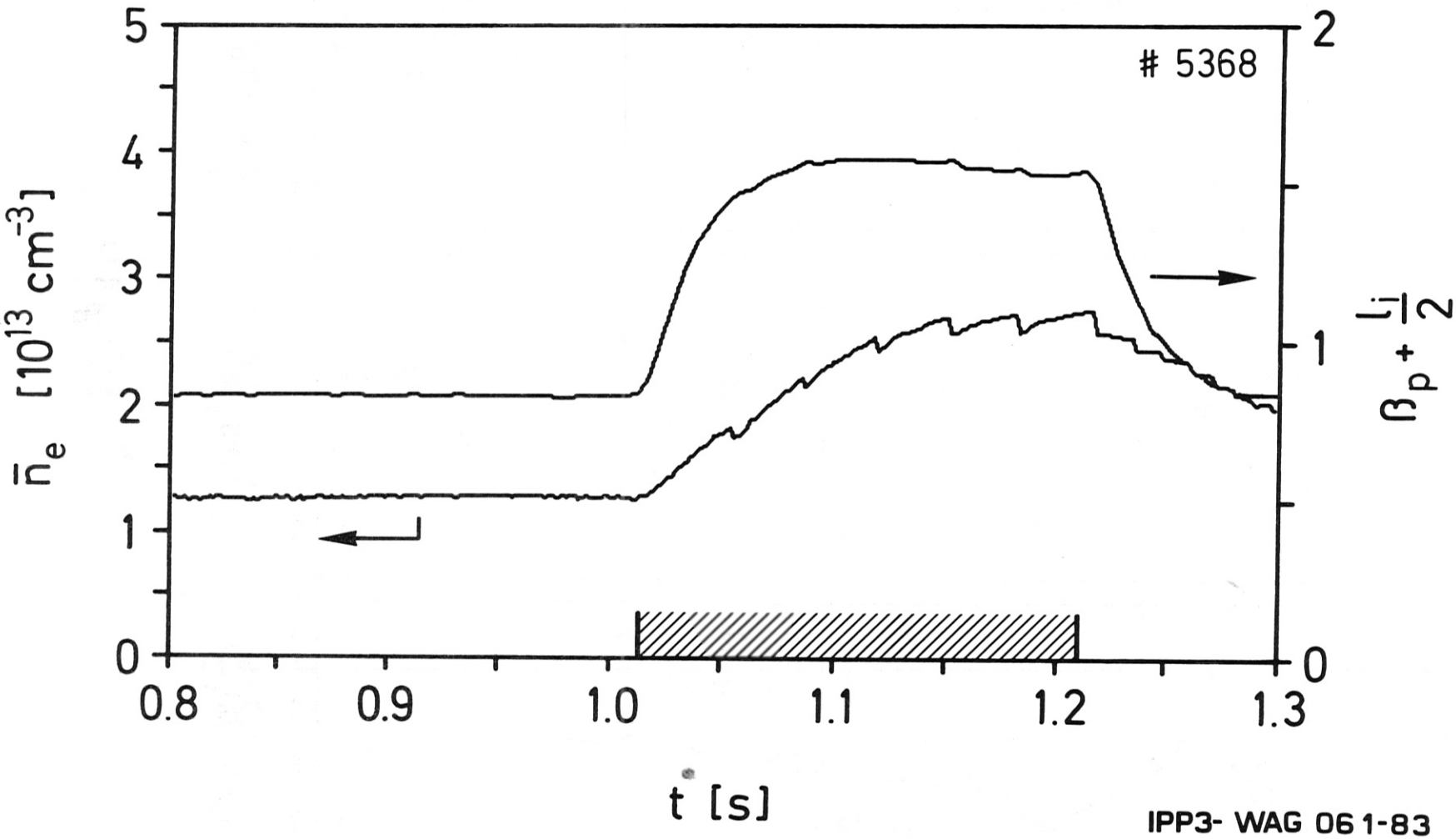
5
4
3
2
1
0
2
1
0
5368
$\bar{n}_e$ [10^{13} cm^{-3}]
$\beta_p + \frac{l_i}{2}$
0.8
0.9
1.0
1.1
1.2
1.3
t [s]
IPP3- WAG 06 1-83

Fig. 7

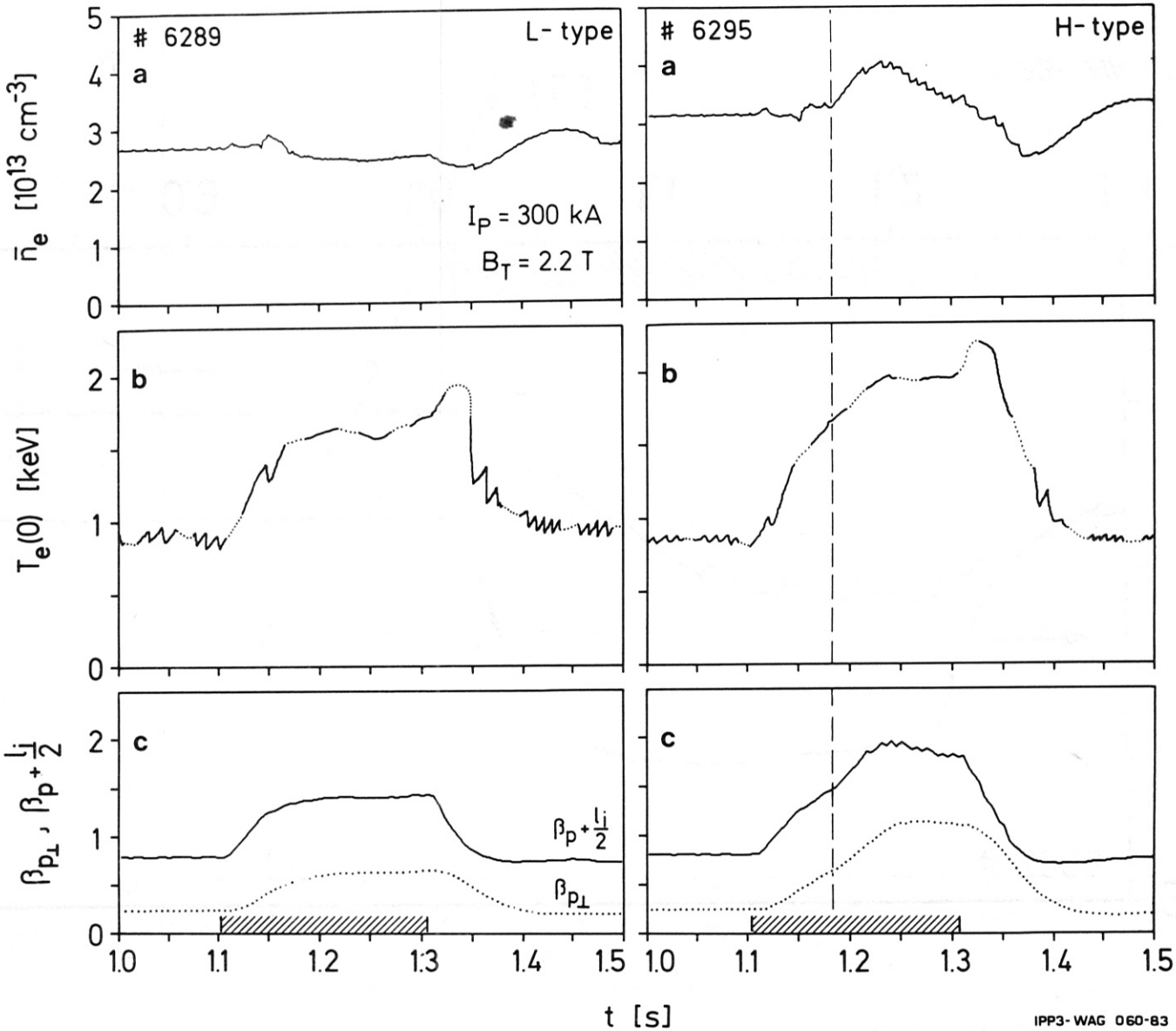
Fig. 8.1
Fig. 8.2
6289
L- type
a
6295
H- type
a
I_P = 300 kA
B_T = 2.2 T
$\bar{n}_e$ [10^{13} cm^{-3}]
b
b
$T_e(0)$ [keV]
c
c
$\beta_{p\perp}$, $\beta_p + \frac{l_i}{2}$
$\beta_p + \frac{l_i}{2}$
$\beta_{p\perp}$
t [s]
IPP3- WAG 060-83

Fig. 8

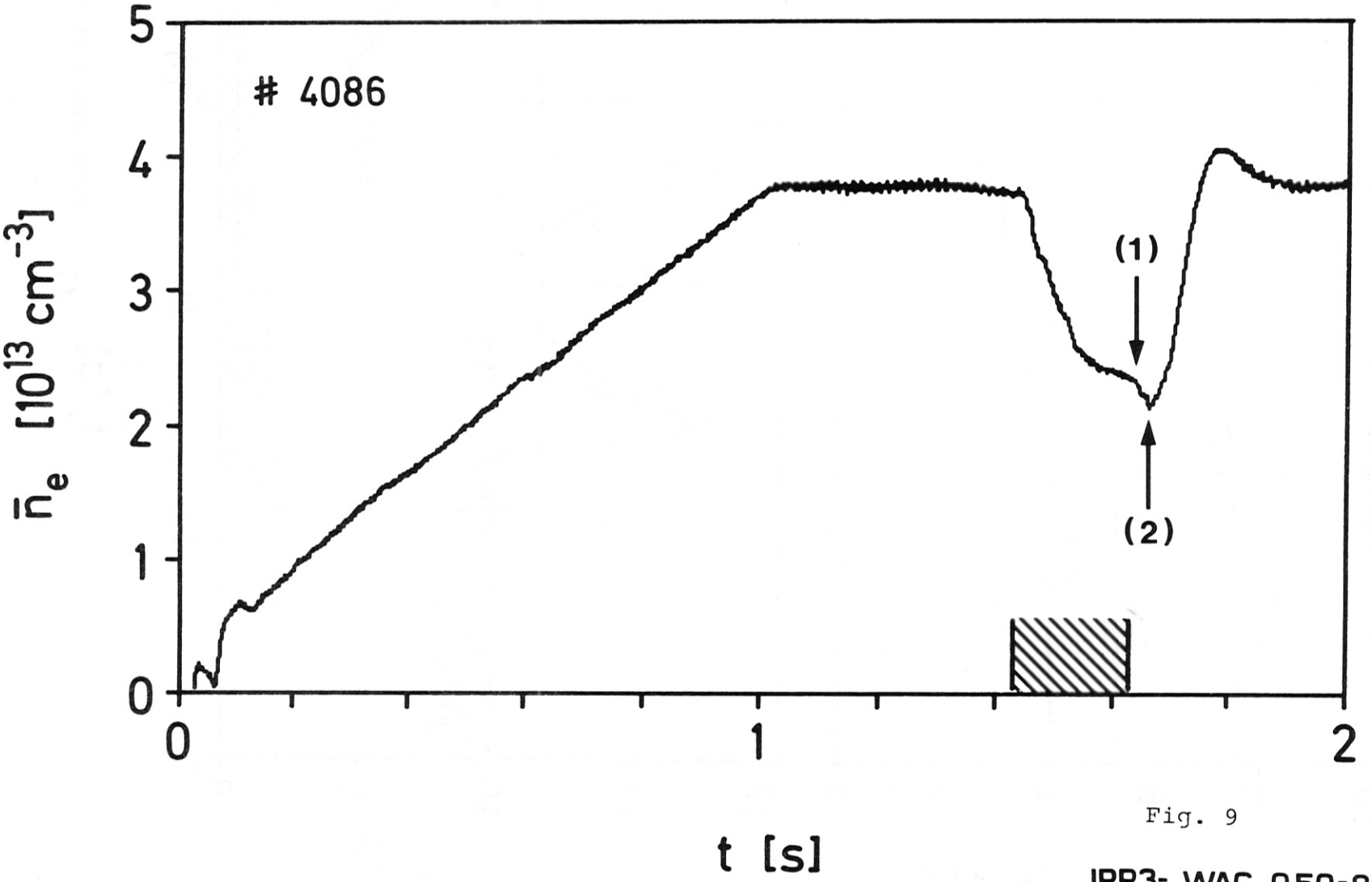

Fig. 9

IPP3- WAG 050-83

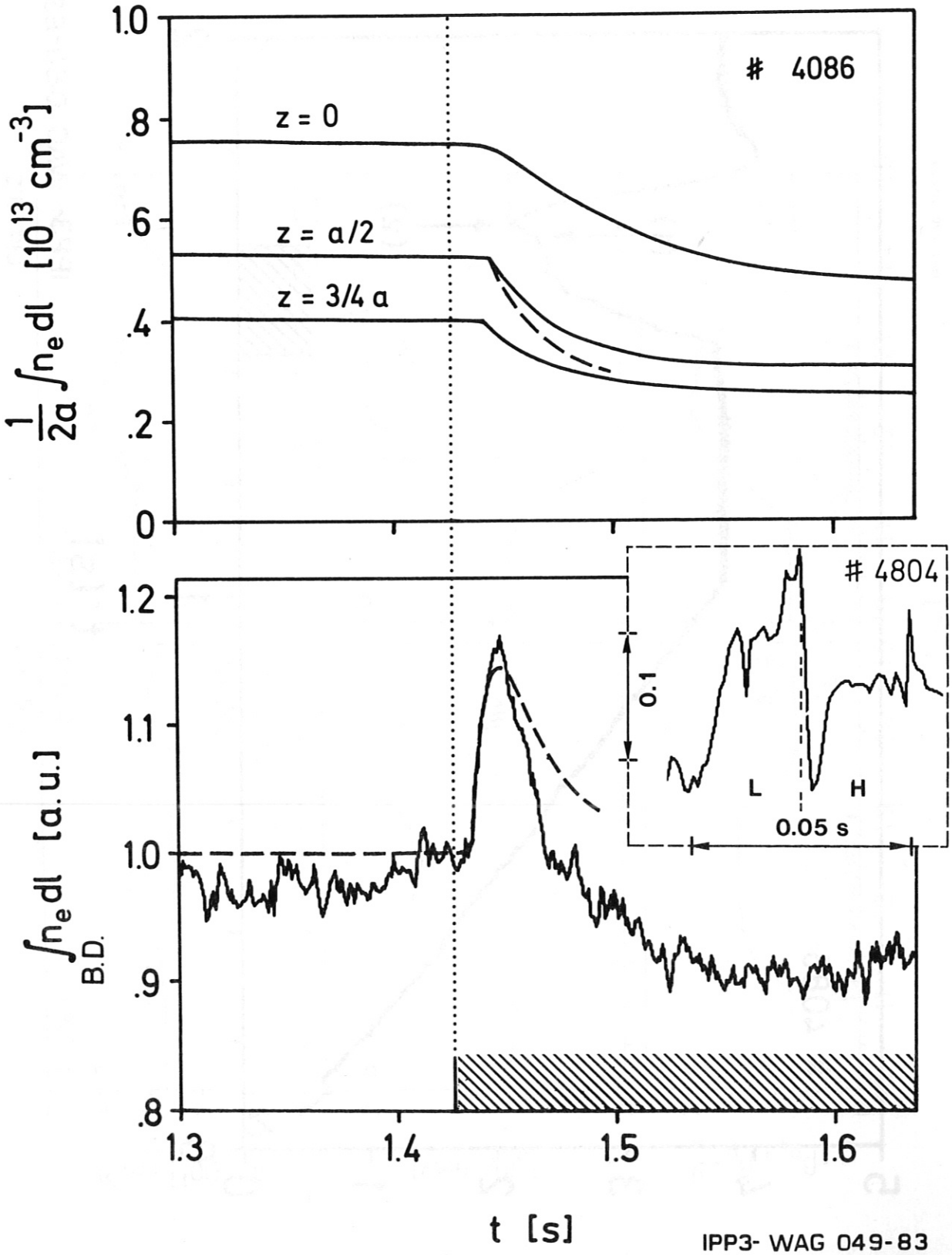

IPP3- WAG 049-83

Fig. 10

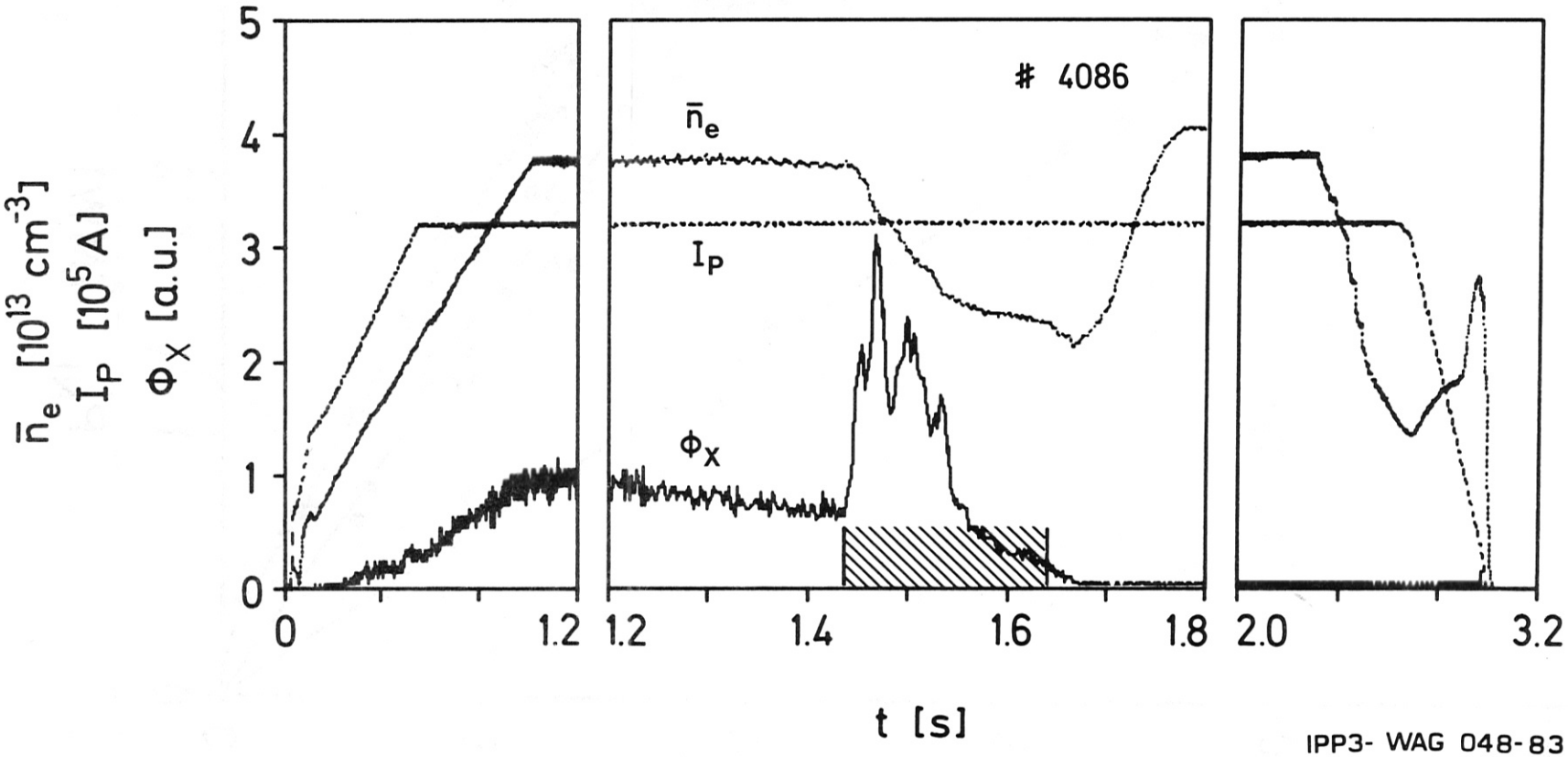

IPP3- WAG 048-83

Fig. 11

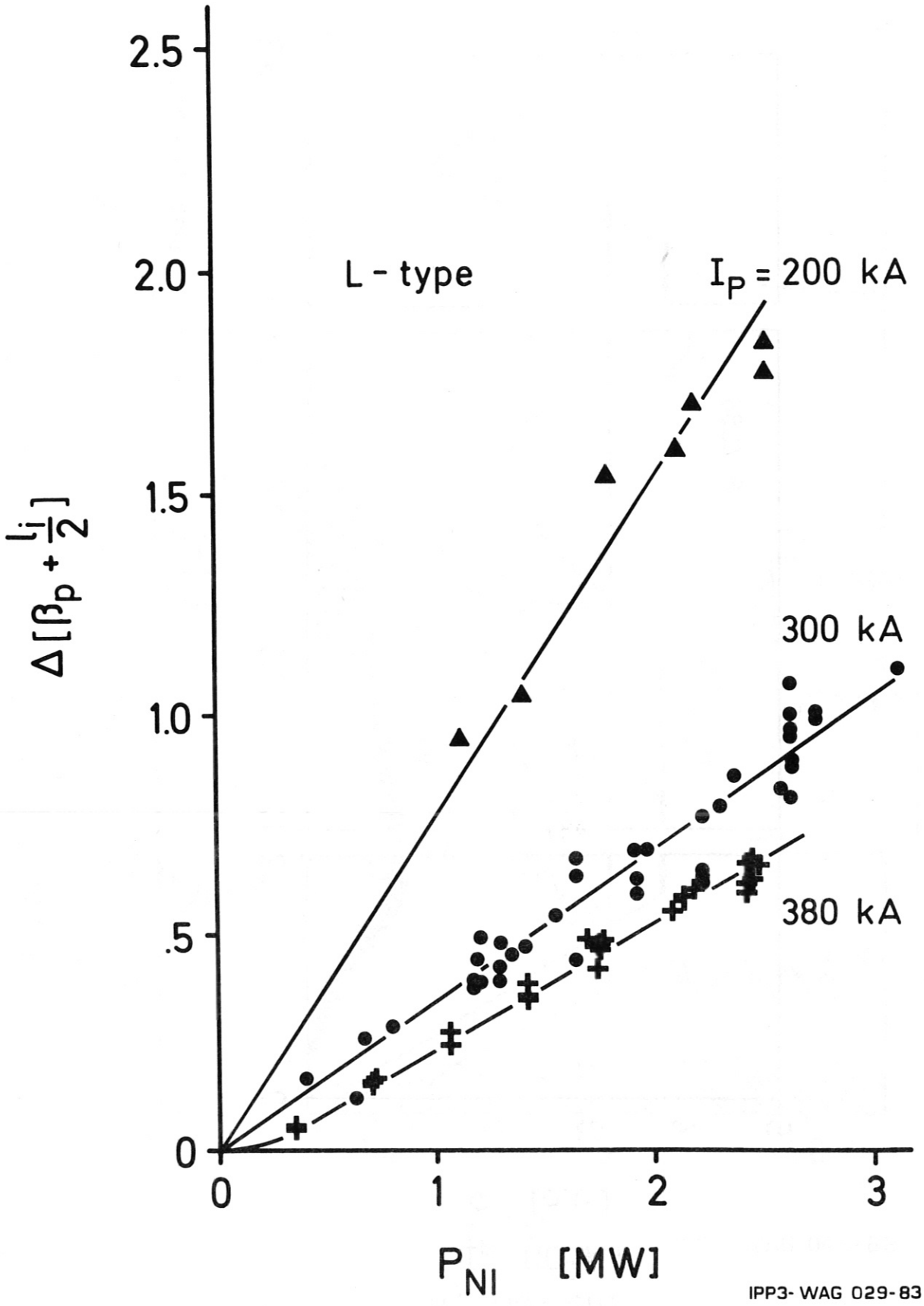
2.5
2.0
1.5
1.0
.5
0
0
1
2
3
L - type
I_P = 200 kA
300 kA
380 kA
$\Delta[\beta_p + \frac{l_i}{2}]$
P_{NI} [MW]
IPP3- WAG 029-83

Fig. 12

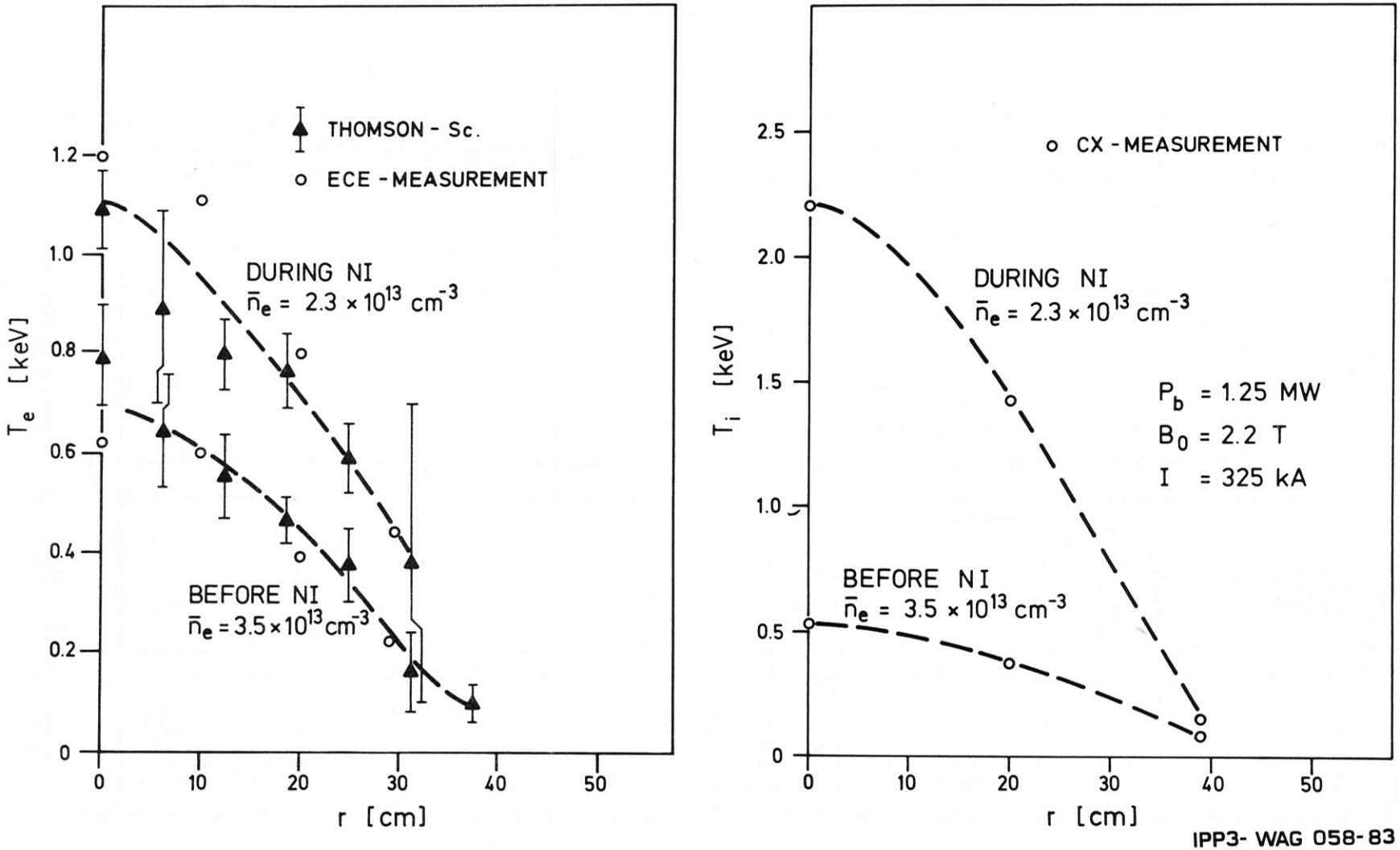
THOMSON - Sc.
ECE - MEASUREMENT
DURING NI
$\bar{n}_e = 2.3 \times 10^{13}\ cm^{-3}$
BEFORE NI
$\bar{n}_e = 3.5 \times 10^{13} cm^{-3}$
T_e [keV]
r [cm]
CX - MEASUREMENT
DURING NI
$\bar{n}_e = 2.3 \times 10^{13}\ cm^{-3}$
P_b = 1.25 MW
B_0 = 2.2 T
I = 325 kA
BEFORE NI
$\bar{n}_e = 3.5 \times 10^{13}\ cm^{-3}$
T_i [keV]
r [cm]
IPP3- WAG 058-83

Fig. 13

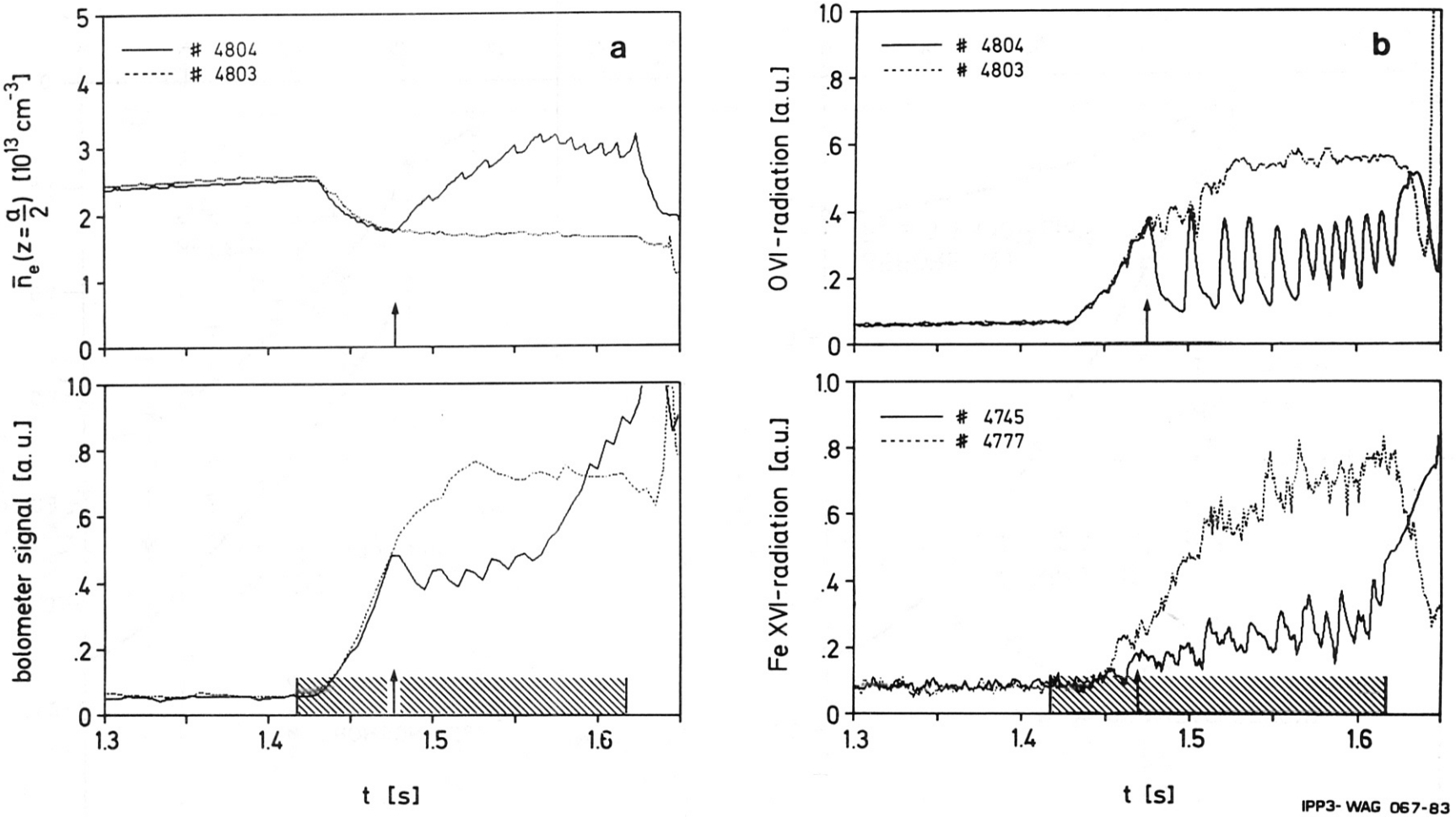
a
4804
4803
$\bar{n}_e(z=\frac{a}{2})$ [10^{13} cm^{-3}]
bolometer signal [a.u.]
t [s]
b
4804
4803
OVI-radiation [a.u.]
4745
4777
Fe XVI-radiation [a.u.]
t [s]
IPP3- WAG 067-83

Fig. 14

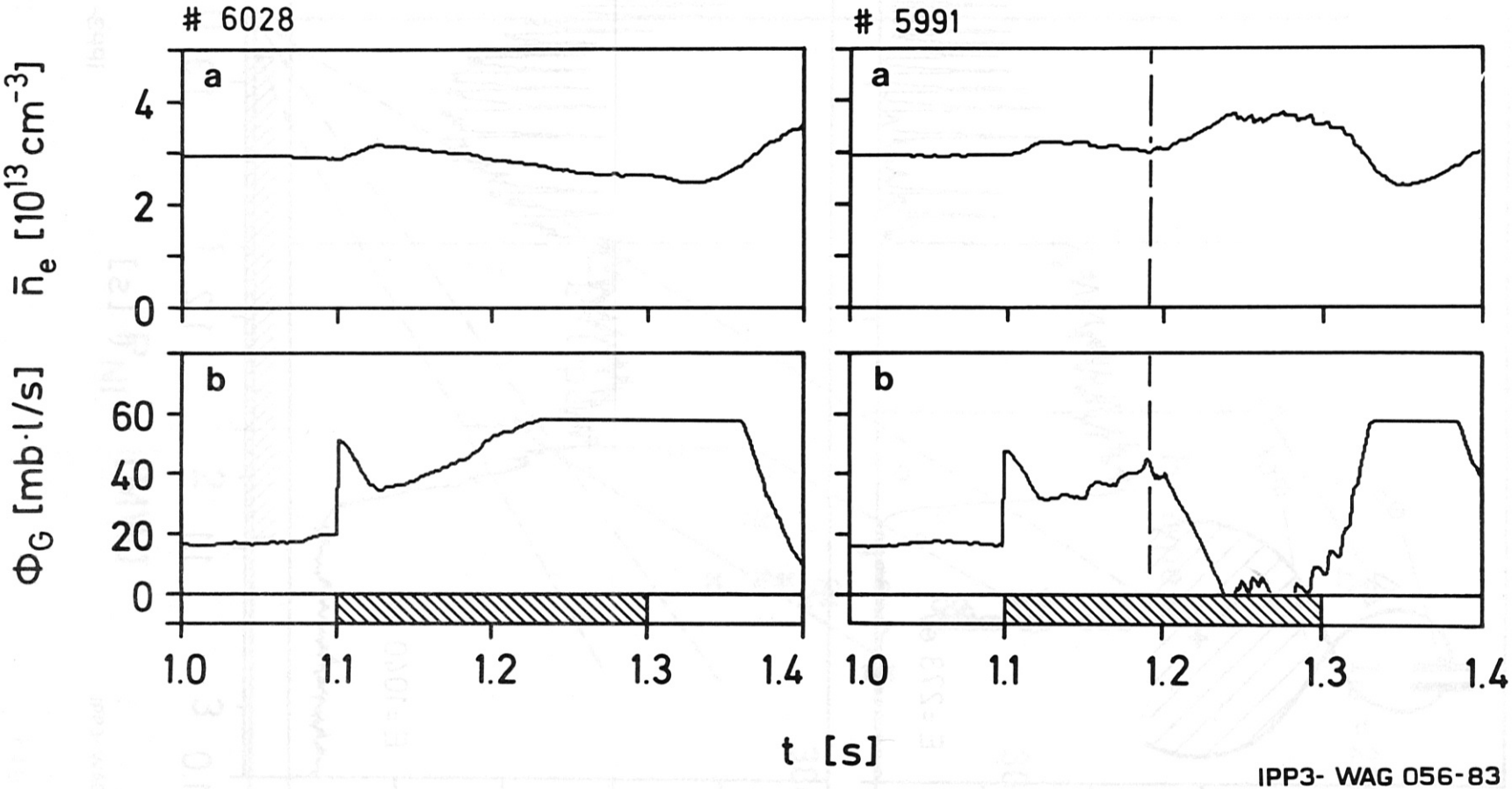

IPP3- WAG 056-83

Fig. 15

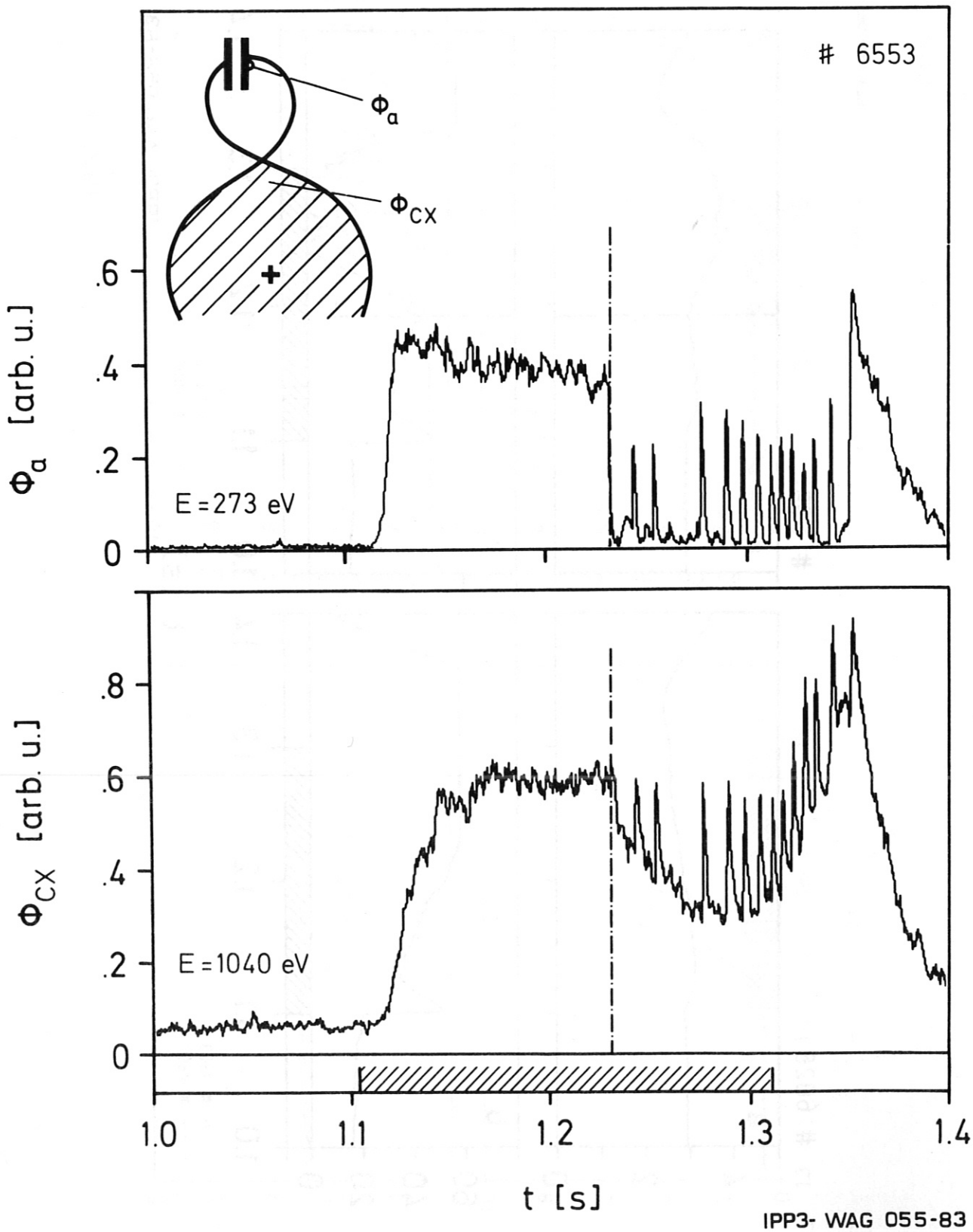
6553
Φ_a
Φ_{CX}
E = 273 eV
E = 1040 eV
Φ_a [arb. u.]
Φ_{CX} [arb. u.]
0
.2
.4
.6
.8
1.0
1.1
1.2
1.3
1.4
t [s]
IPP3- WAG 055-83

Fig. 16

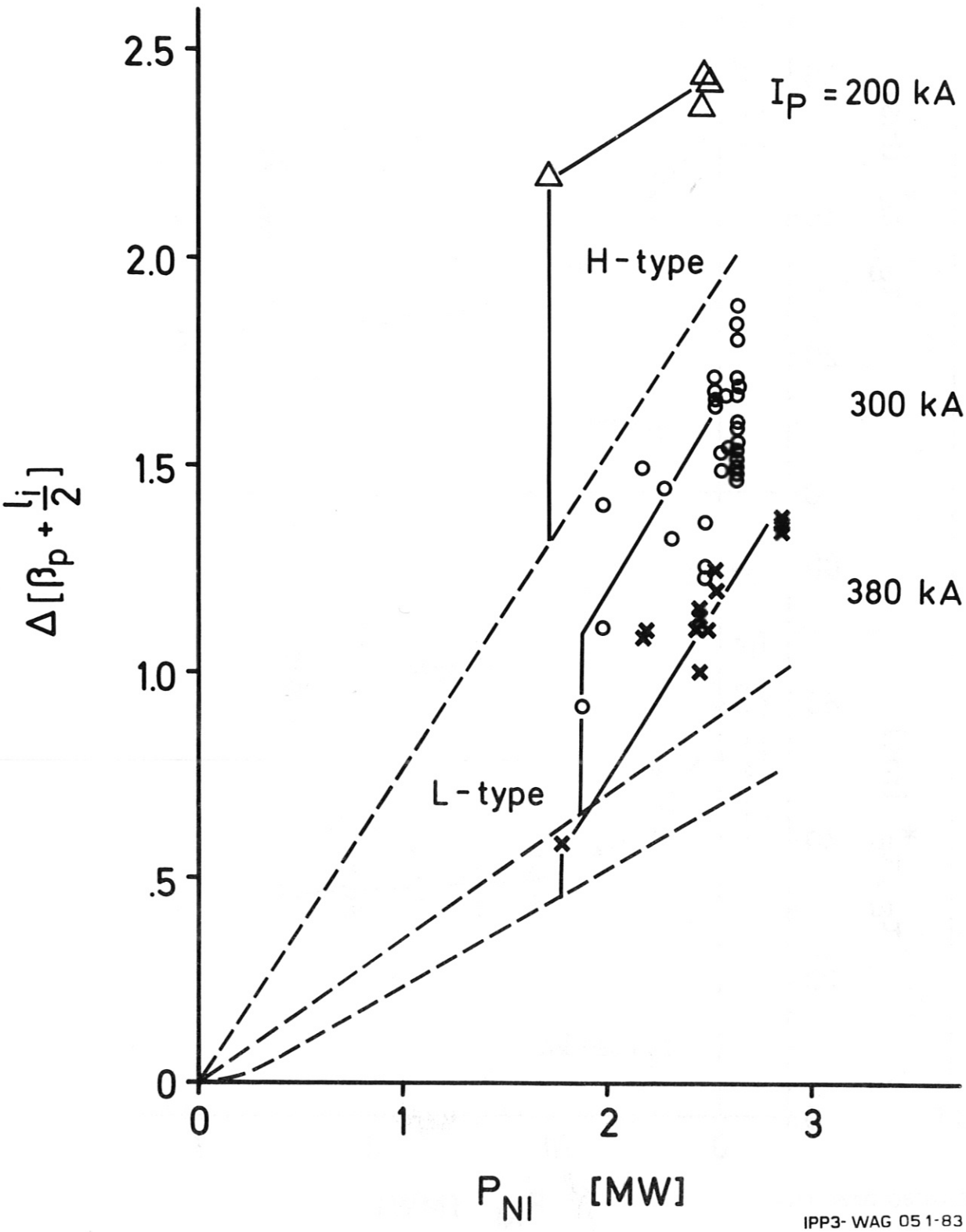
2.5
2.0
1.5
1.0
.5
0
0
1
2
3
$\Delta[\beta_p + \frac{l_i}{2}]$
P_{NI} [MW]
I_P = 200 kA
H-type
300 kA
380 kA
L-type
IPP3- WAG 051-83

Fig. 17

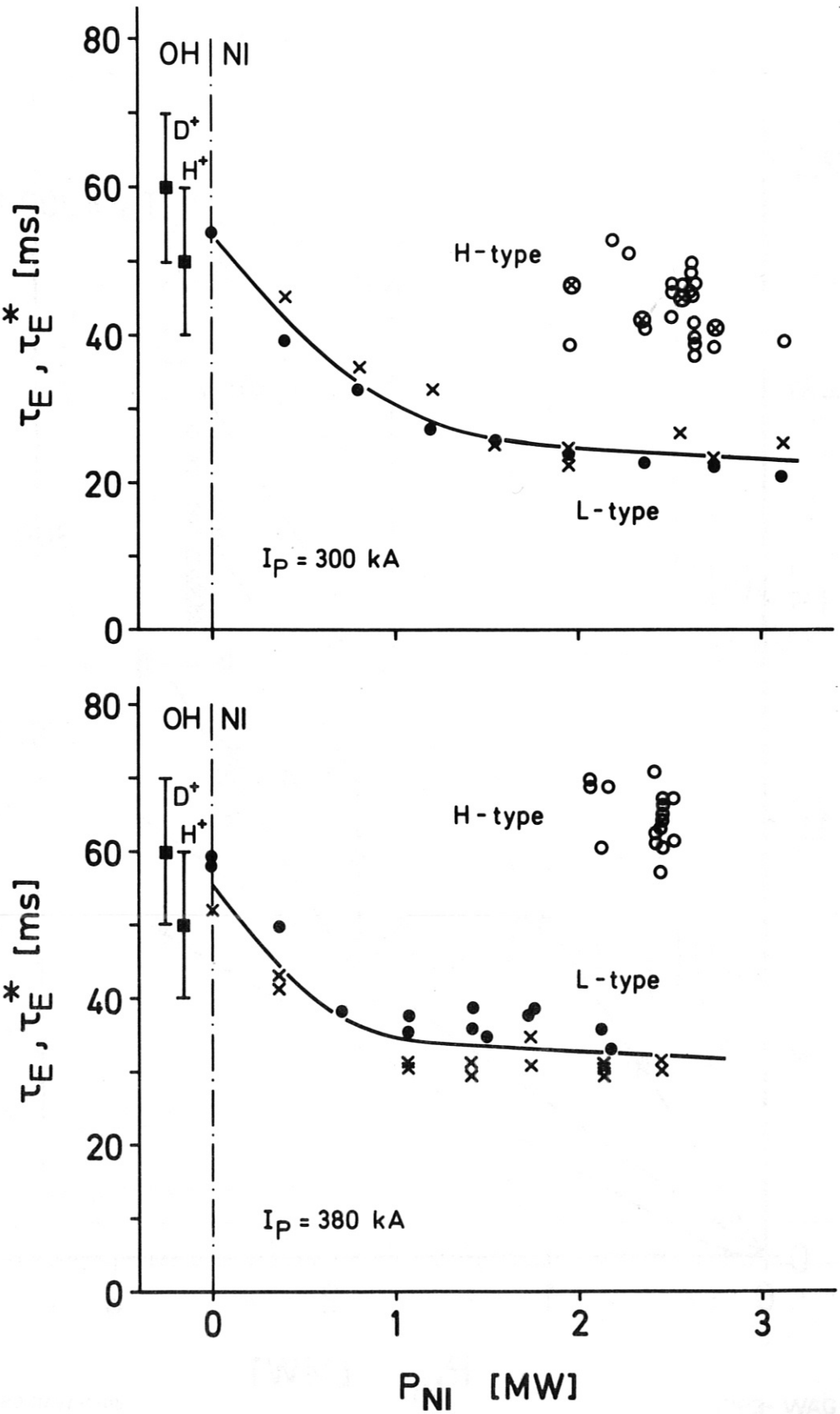

IPP3- WAG 442-82

Fig. 18

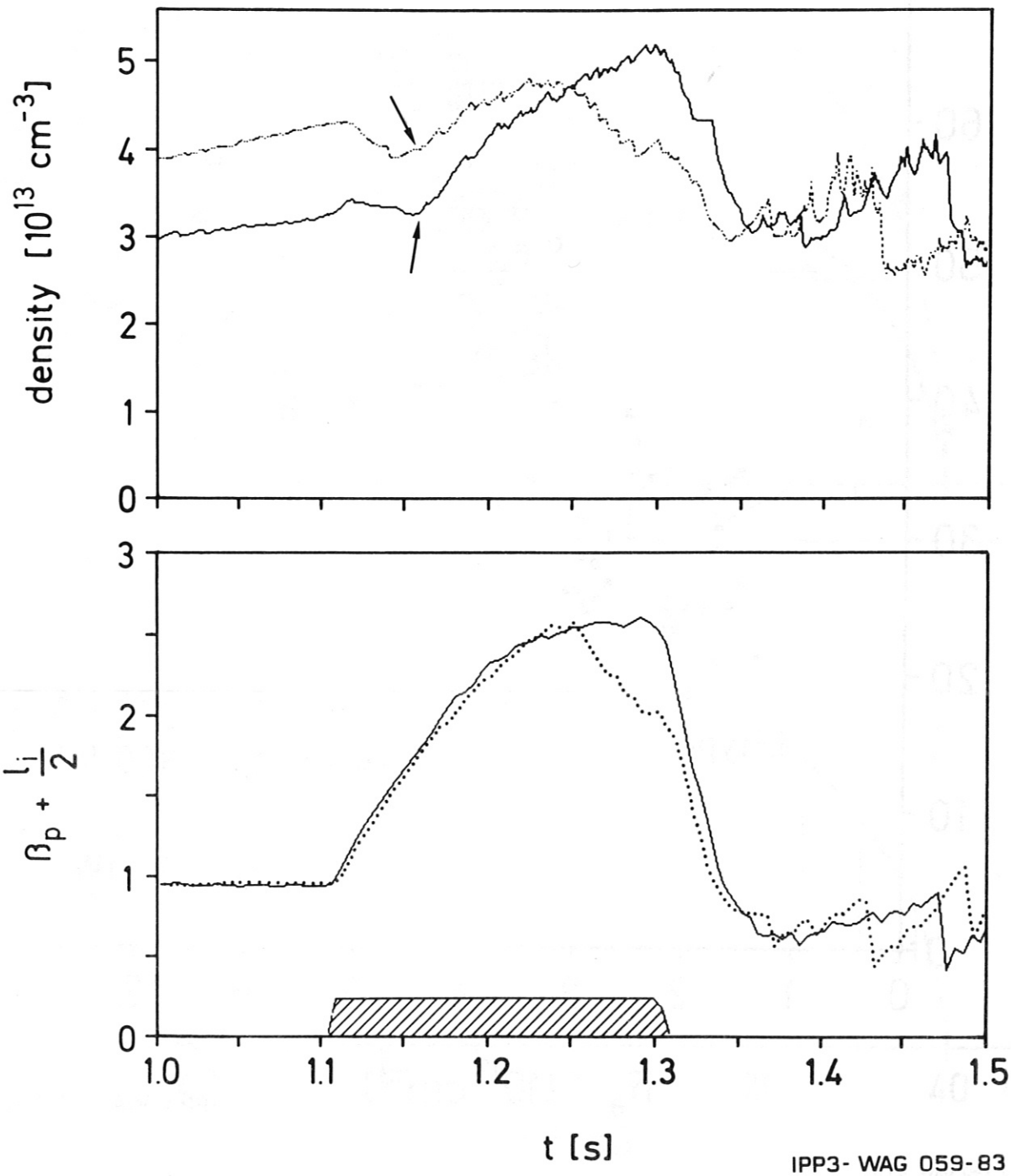
density [10^{13} cm^{-3}]
0
1
2
3
4
5
$\beta_p + \frac{l_i}{2}$
0
1
2
3
1.0
1.1
1.2
1.3
1.4
1.5
t [s]
IPP3- WAG 059-83

Fig. 19

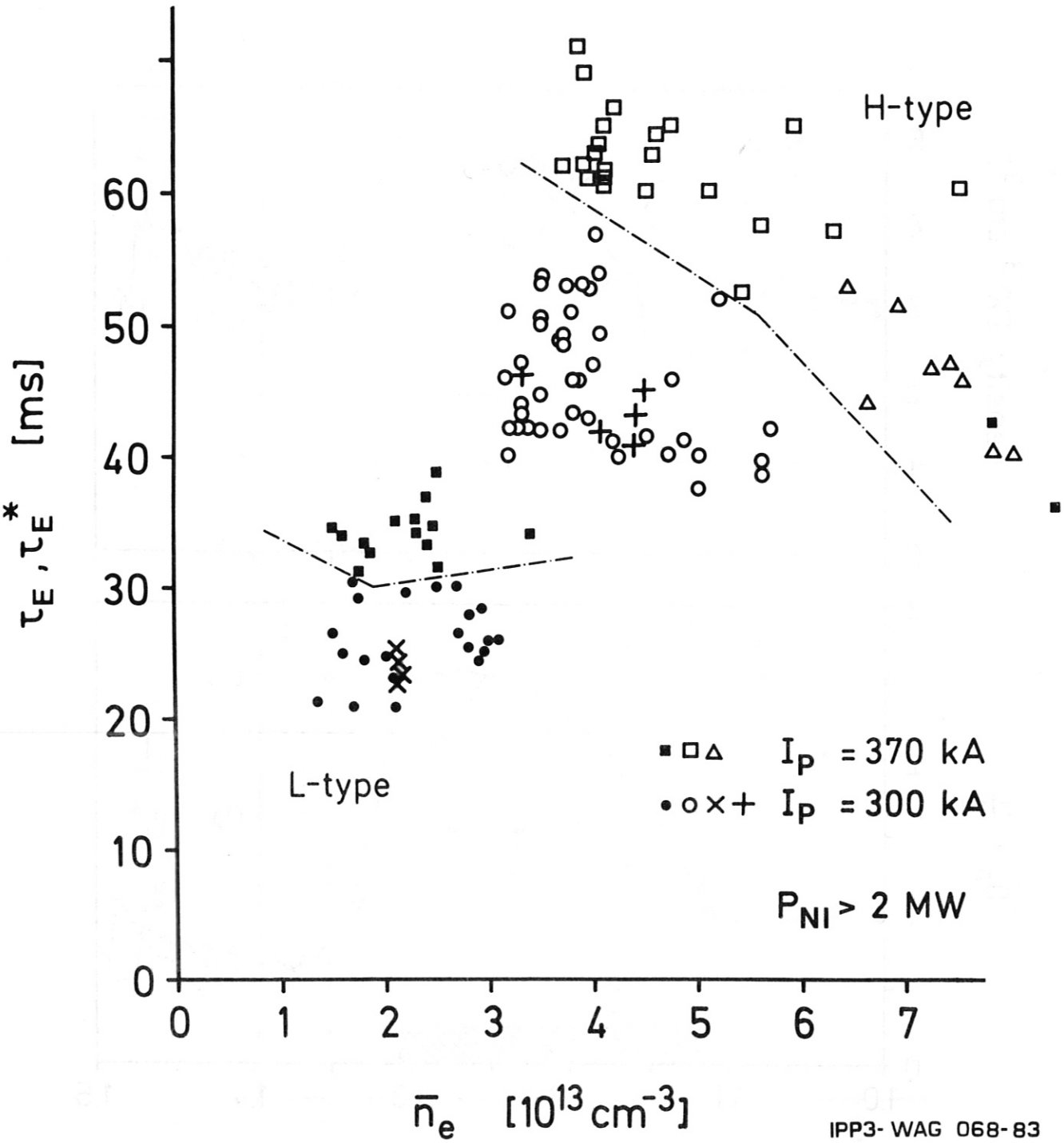
H-type
L-type
I_P = 370 kA
I_P = 300 kA
P_{NI} > 2 MW
τ_E, τ_E^* [ms]
$\bar{n}_e$ [10^{13} cm^{-3}]
0
10
20
30
40
50
60
0
1
2
3
4
5
6
7
IPP3- WAG 068-83

Fig. 20

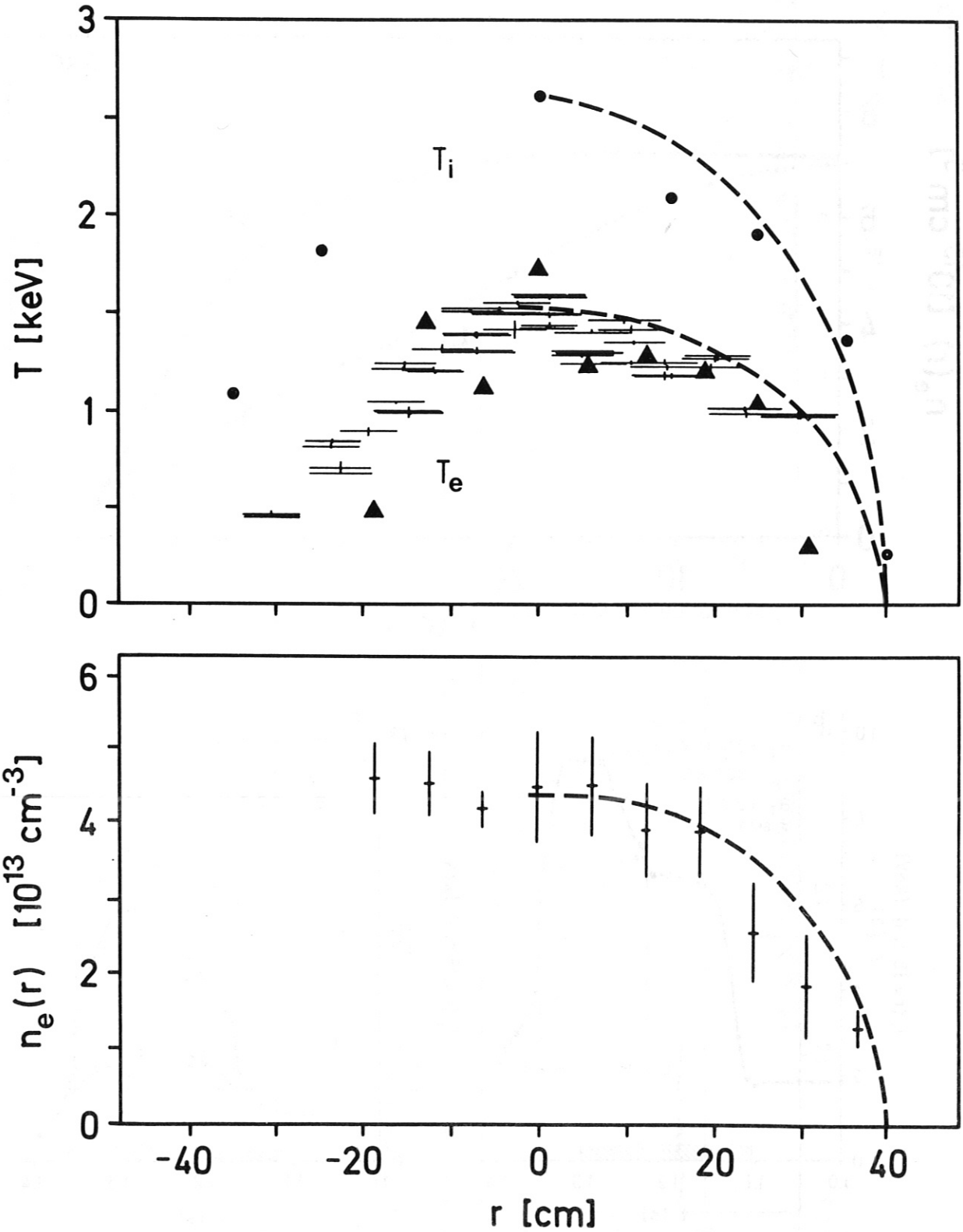

Fig. 21

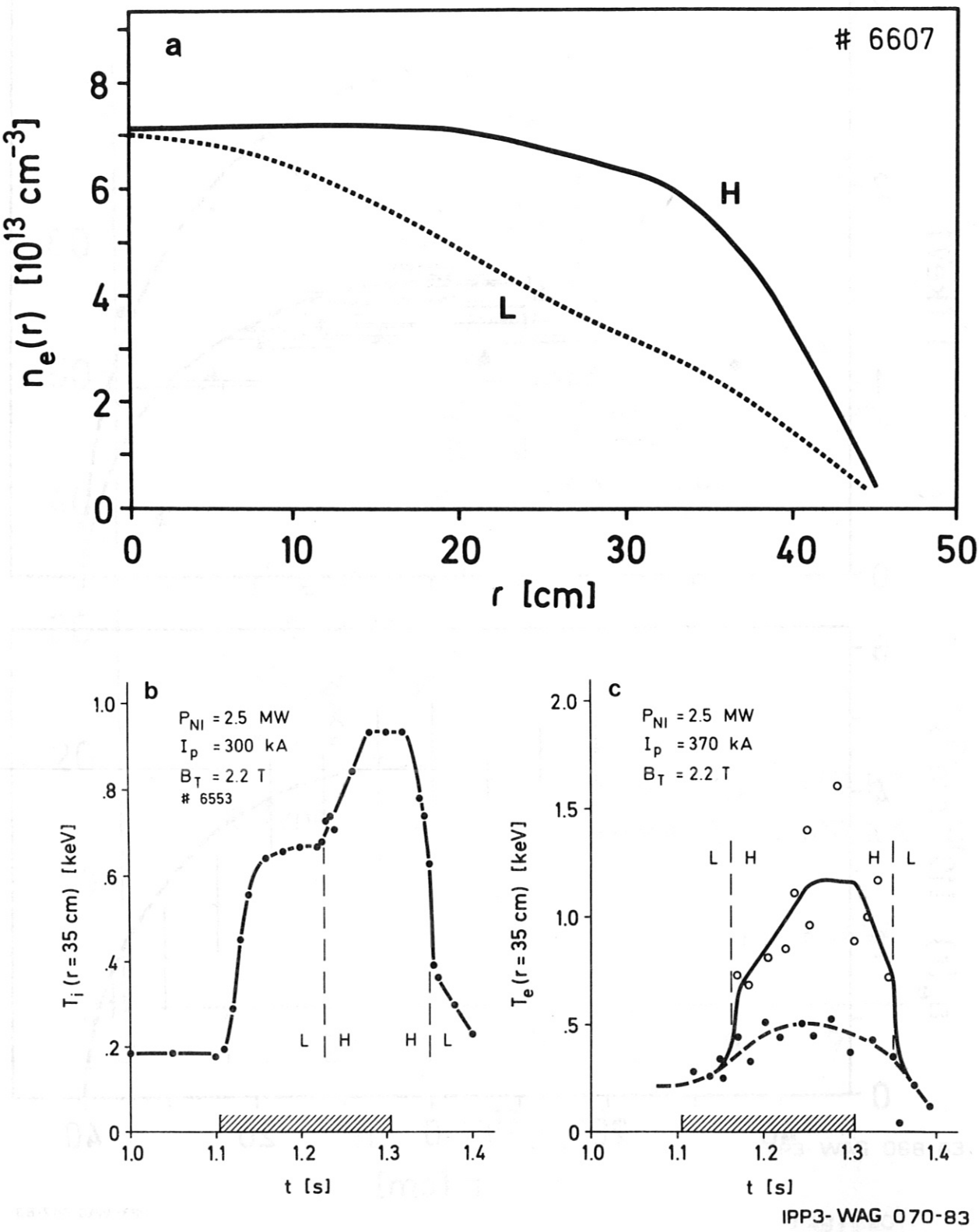
a
6607
H
L
$n_e(r)$ [10^{13} cm^{-3}]
r [cm]
b
P_{NI} = 2.5 MW
I_p = 300 kA
B_T = 2.2 T
6553
T_i (r = 35 cm) [keV]
t [s]
c
P_{NI} = 2.5 MW
I_p = 370 kA
B_T = 2.2 T
T_e (r = 35 cm) [keV]
t [s]
IPP3- WAG 070-83

Fig. 22

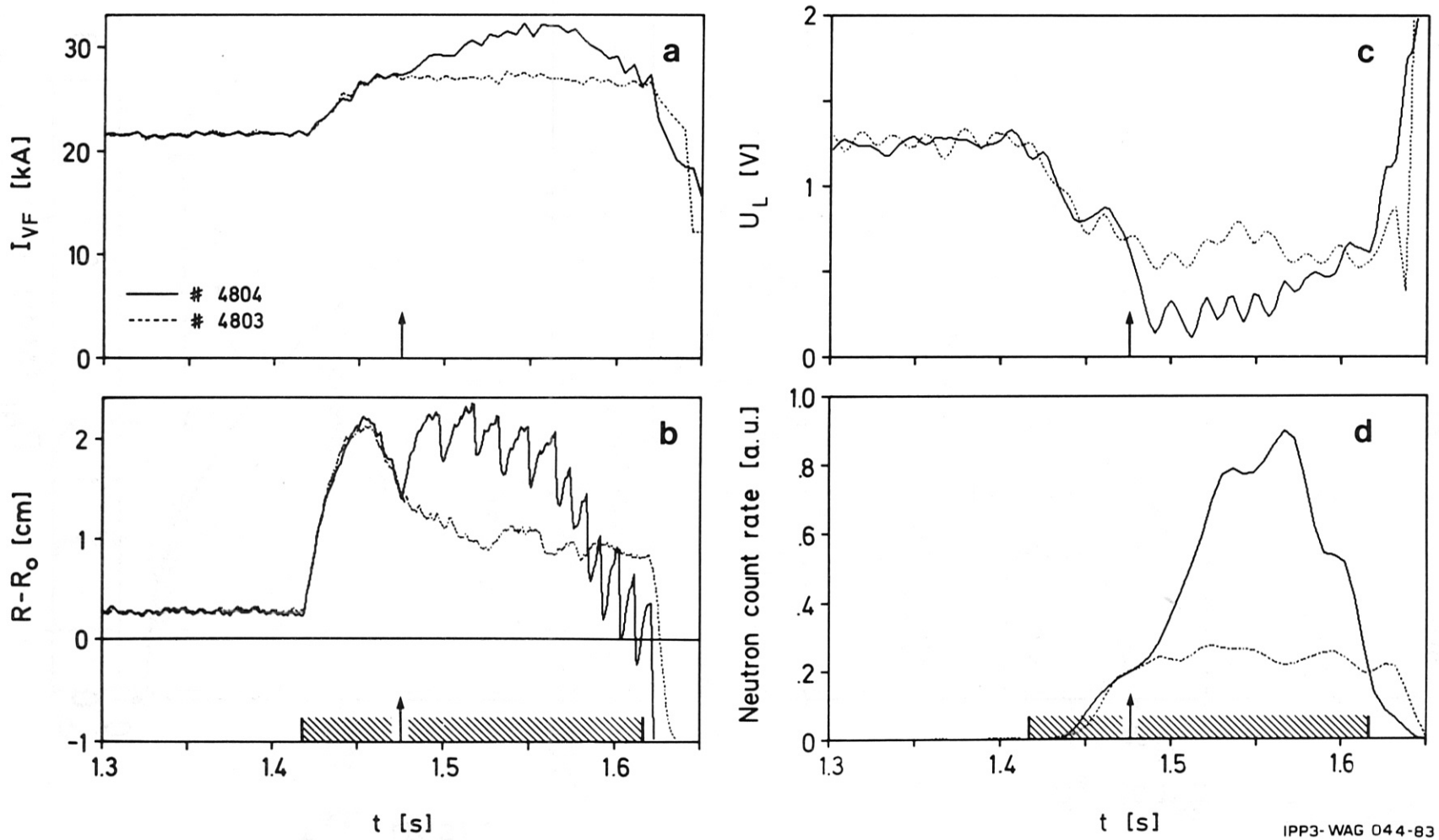
a
b
c
d
I_{VF} [kA]
R-R_o [cm]
U_L [V]
Neutron count rate [a.u.]
4804
4803
t [s]
t [s]
IPP3-WAG 044-83

Fig. 23

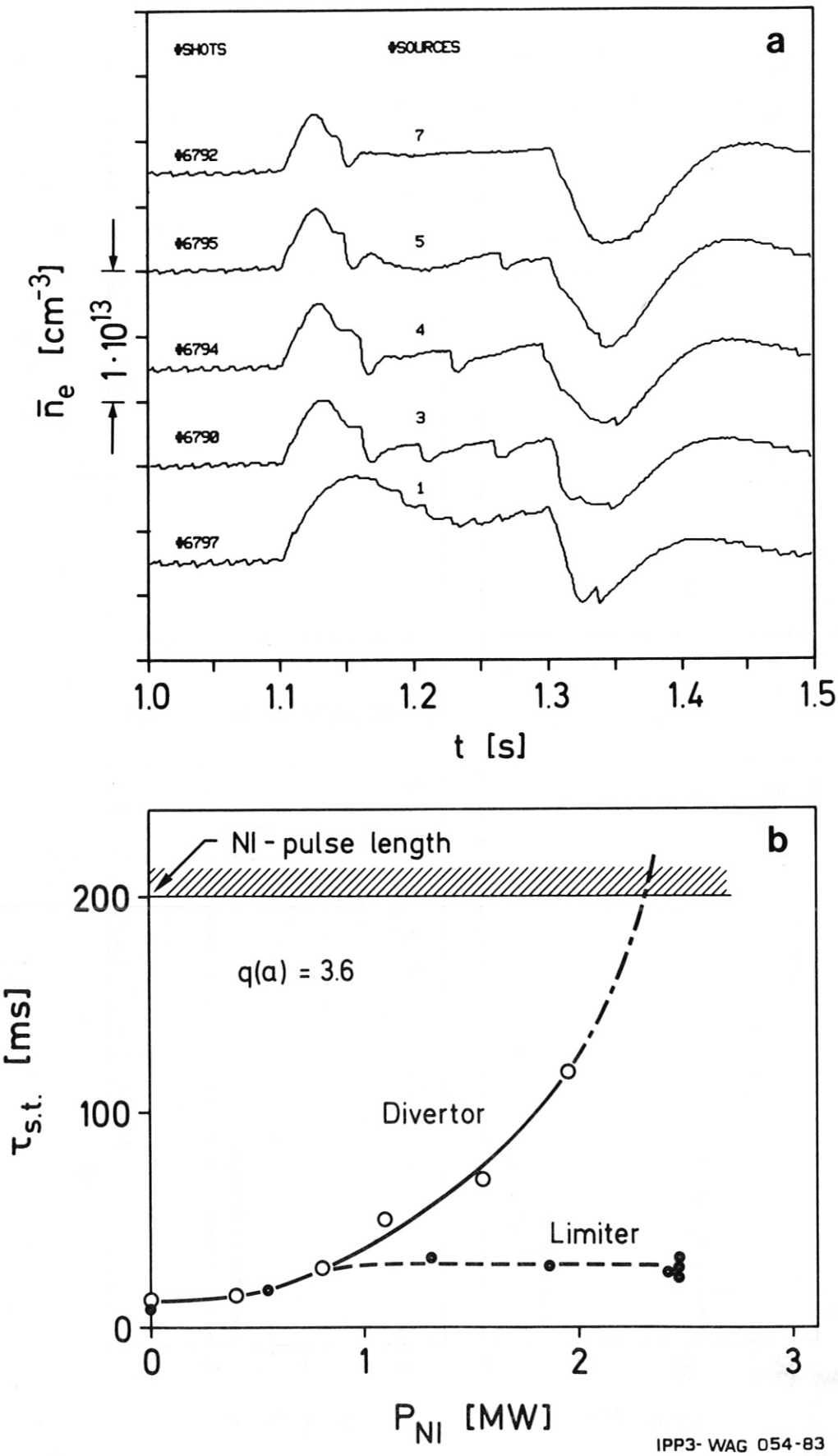
#SHOTS
#SOURCES
a
#6792
7
#6795
5
#6794
4
#6790
3
#6797
1
$\bar{n}_e$ [cm^{-3}]
$1 \cdot 10^{13}$
1.0
1.1
1.2
1.3
1.4
1.5
t [s]
b
NI - pulse length
200
100
0
q(a) = 3.6
Divertor
Limiter
$\tau_{s.t.}$ [ms]
0
1
2
3
P_{NI} [MW]
IPP3- WAG 054-83

Fig. 24

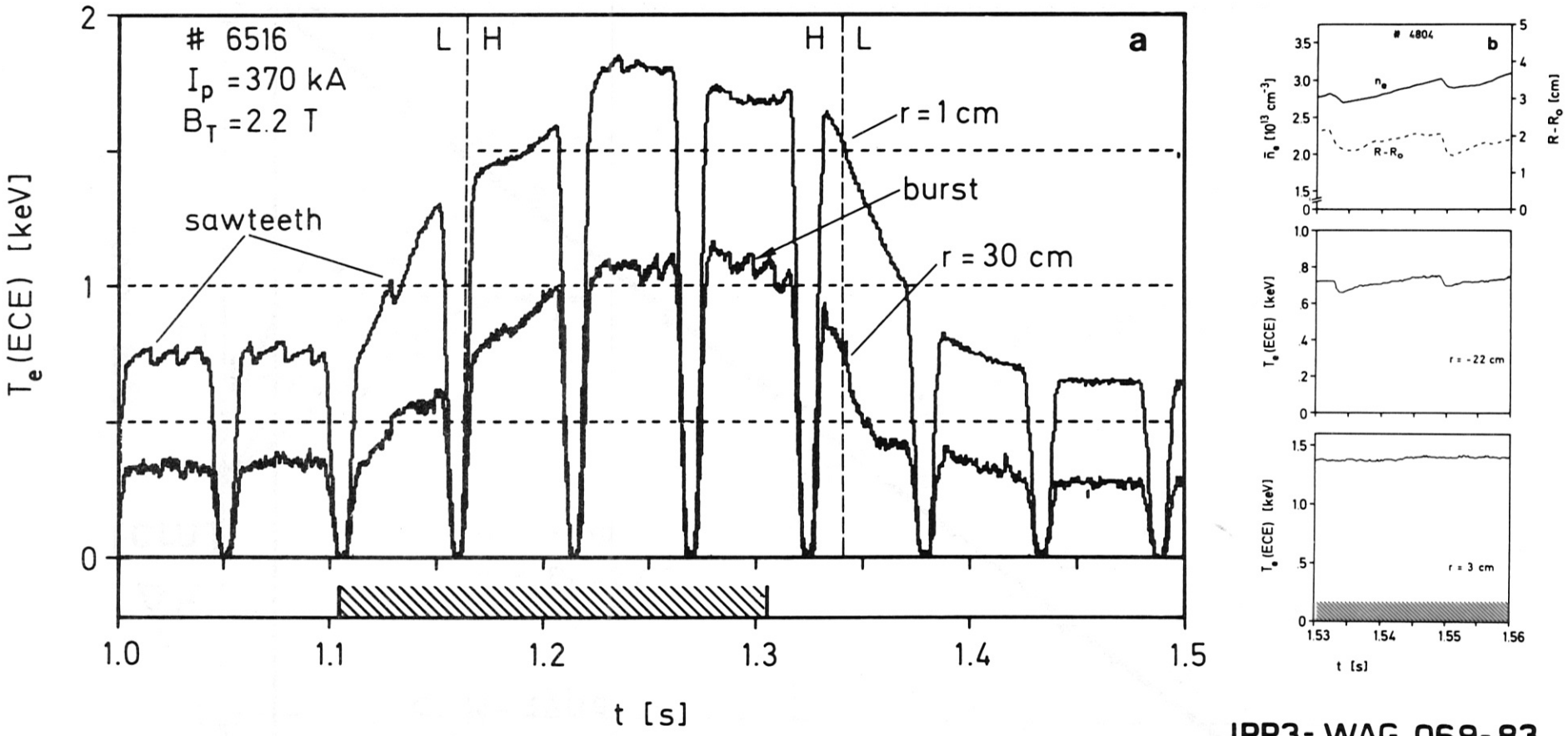

IPP3- WAG 069-83

Fig. 25

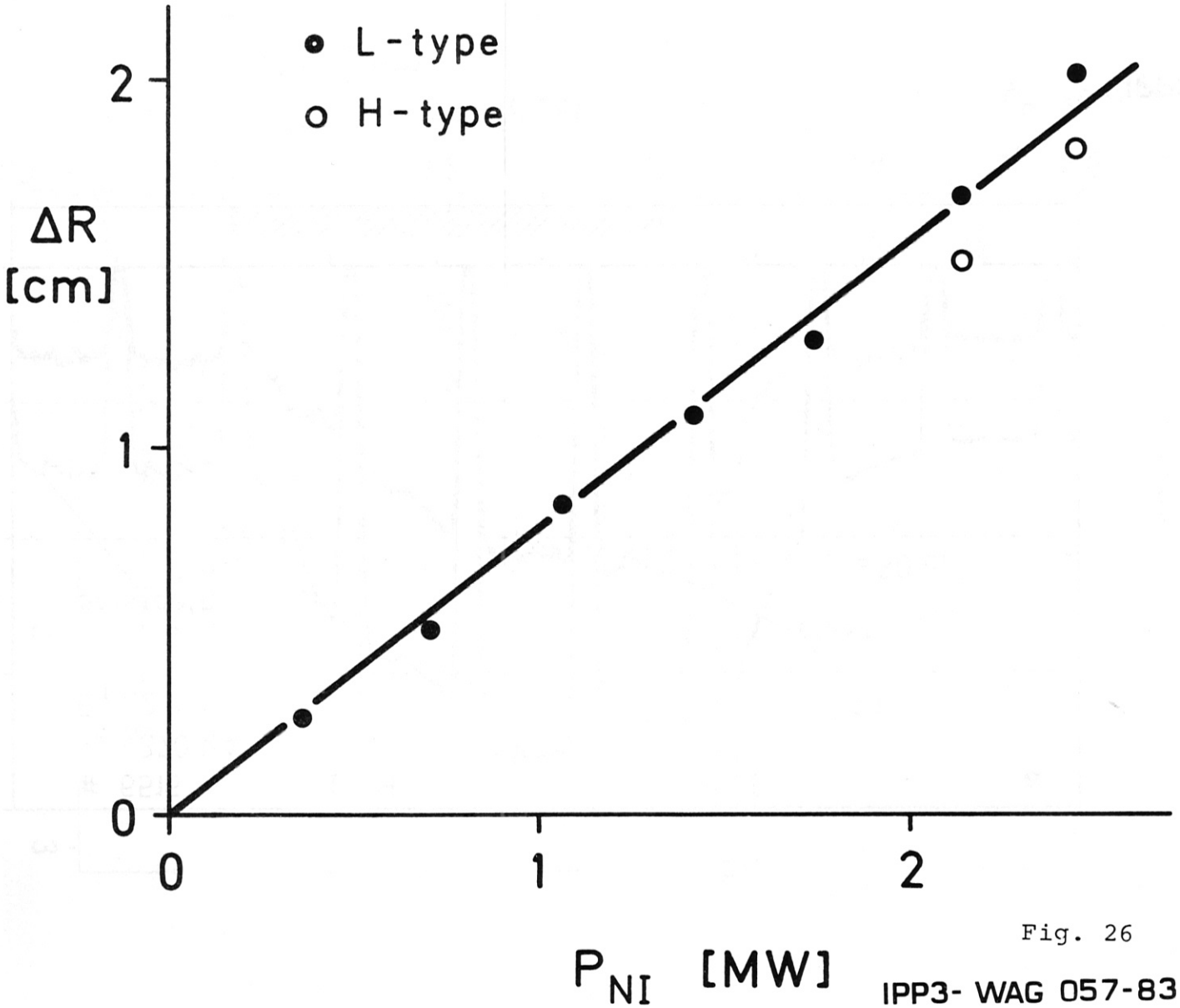

Fig. 26

IPP3- WAG 057-83

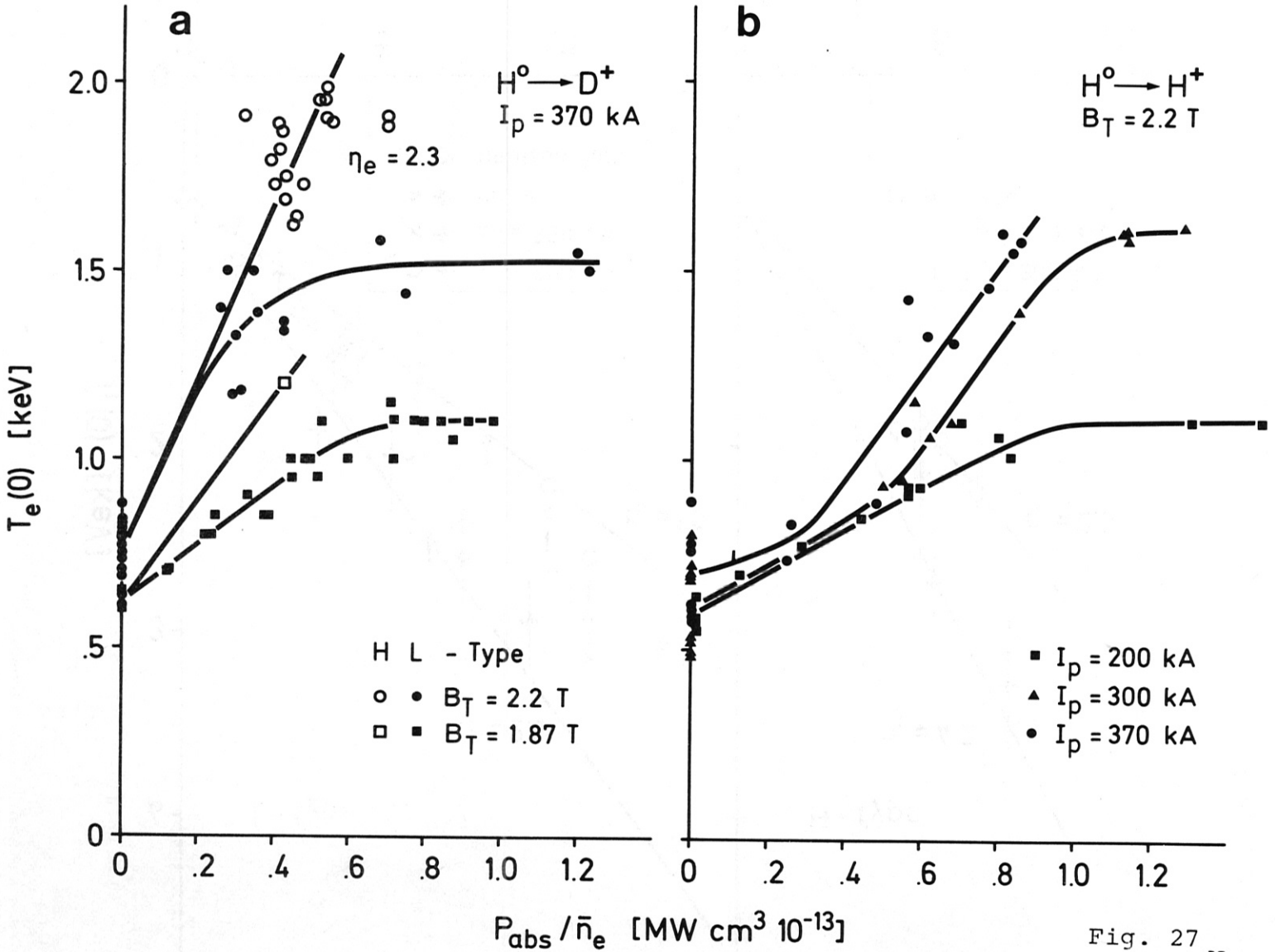
a
b
$H^o \rightarrow D^+$
I_p = 370 kA
8
η_e = 2.3
$H^o \rightarrow H^+$
B_T = 2.2 T
H L - Type
B_T = 2.2 T
B_T = 1.87 T
I_p = 200 kA
I_p = 300 kA
I_p = 370 kA
$T_e(0)$ [keV]
$P_{abs}/\bar{n}_e$ [MW cm^3 10^{-13}]
0
.5
1.0
1.5
2.0
.2
.4
.6
.8
1.2

Fig. 27

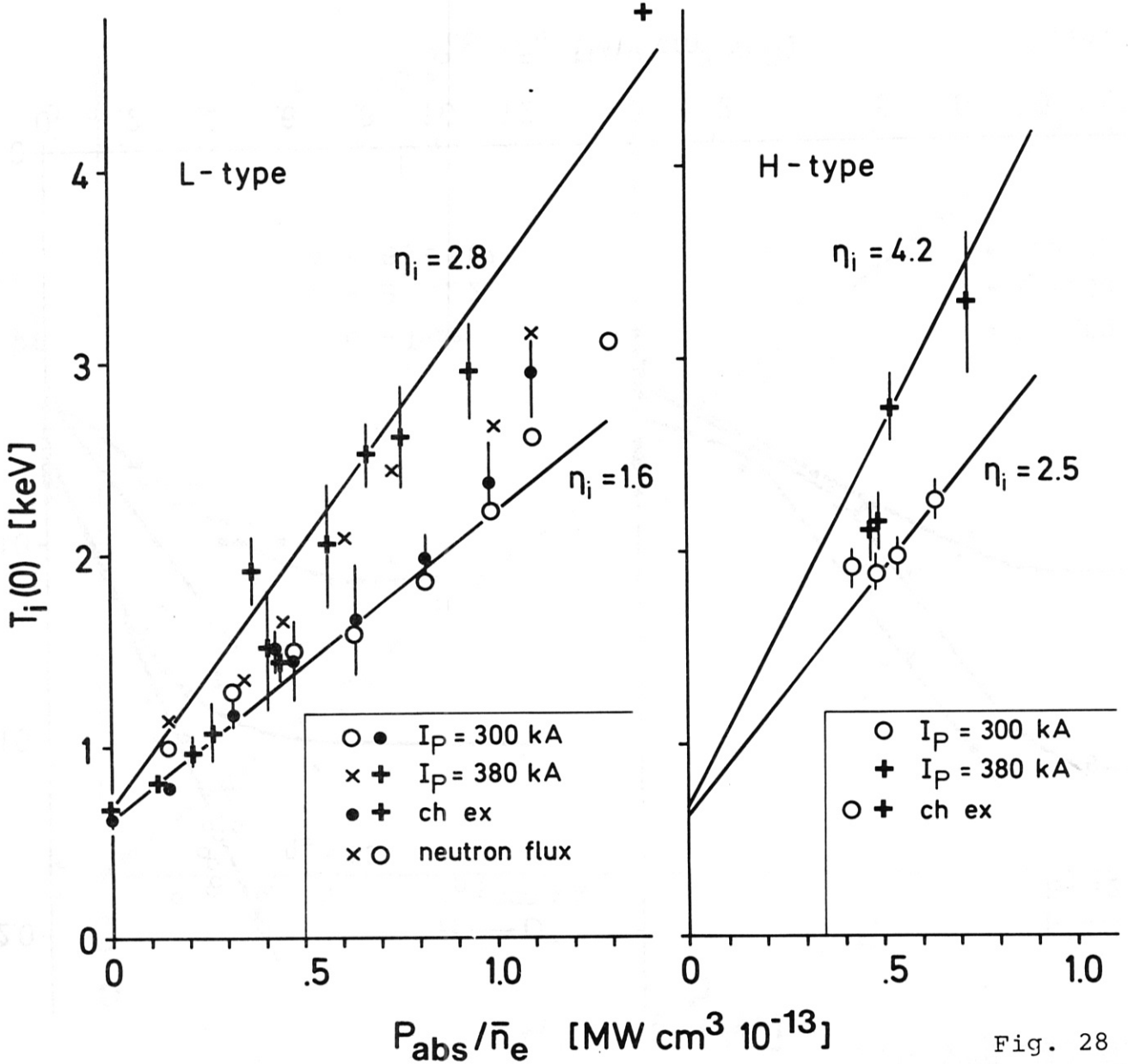
L - type
H - type
η_i = 2.8
η_i = 1.6
η_i = 4.2
η_i = 2.5
I_P = 300 kA
I_P = 380 kA
ch ex
neutron flux
$T_i(0)$ [keV]
$P_{abs}/\bar{n}_e$ [MW cm^3 10^{-13}]
0
1
2
3
4
.5
1.0

Fig. 28